Journal of Molecular Structure 1340 (2025) 142549

Contents lists available at ScienceDirect

Journal of Molecular Structure

journal homepage: www.elsevier.com/locate/molstr

Novel 3-aminoimidazole[1,2-α]pyridine/pyrazine analogues: Synthesis and biological evaluation as anticancer agents

Isra' Al-Qadi [a], Michel Hanania [b], Saied M Soliman [c], Nurul Izzaty Hassan [d], Wan Nurfadhilah Zaharim [d], Saki Raheem [e,*], Nawaf Al-Maharik [a,*]

[a] Department of Chemistry, Faculty of Science, An-Najah National University, Nablus, 00970, Palestine
[b] Department of Chemistry, Faculty of Applied Sciences, Technology and Engineering, Bethlehem University, Bethlehem, 00970, Palestine
[c] Department of Chemistry, Faculty of Science, Alexandria University, Alexandria, 21511, Egypt
[d] Department of Chemical Sciences, Faculty of Science & Technology, Universiti Kebangsaan Malaysia, Bandar Baru Bangi, Selangor, 43600, Malaysia
[e] School of Life Science, University of Westminster, 115 New Cavendish Street, London, W1W 6UW, UK

ARTICLE INFO

Keywords:
3-Aminoimidazo[1,2-α]pyridines/pyrazines
Anticancer
GBB-3CR

ABSTRACT

Herein, we report the synthesis of novel derivatives of 3-aminoimidazole[1,2-α]pyridine/pyrazines via a one-pot Groebke-Blackburn-Bienayme Three-Component Reaction (GBB-3CR) as promising anticancer agents. The synthesised compounds were evaluated for efficacy against three cancer cell lines (MCF-7, HT-29, and B16F10) and one normal cell (MEF). Among the thirteen compounds tested, only compounds **16** and **18** significantly inhibited cancer cells, with high selectivity. Compound **16** showed strong activity against HT-29 ($IC_{50} = 12.98 \pm 0.40$ μM) and B16F10 ($IC_{50} = 27.54 \pm 1.26$ μM), whereas compound **18**, bearing a 2,4-difluorophenyl substitution at C-2 and a *p*-fluorophenyl amine at C-3, was most effective against MCF-7 ($IC_{50} = 9.60 \pm 3.09$ μM). X-ray crystallographic analysis for compounds **9** and **20** confirmed their molecular structures and revealed significant differences in twist angles (87.59° in **9** vs 75.65° in **20**) and π-π stacking interactions (C…C: 3.206-3.394 Å). Hirshfeld surface analysis highlighted key intermolecular forces governing crystal packing, with potential implications for solubility, stability, and molecular interactions with biological targets. Density functional theory (DFT) calculations further suggested that compound 18's larger HOMO-LUMO gap enhances electronic stability and molecular recognition, contributing to its selective cytotoxicity. These findings highlight the structural and electronic factors influencing the anticancer activity of imidazo[1,2-α]pyridine/pyrazine derivatives and provide insights for further optimisation of their therapeutic potential.

1. Introduction

According to a report by the International Agency for Research on Cancer (IARC)), cancer caused nearly 10 million deaths globally in 2022 [1]. Despite the development of innovative treatments over the past decade, cancer continues to be a significant global health issue [2–8]. The rising incidence of cancer and increasing resistance to targeted drugs [3,4] underscores the importance of developing new medicines. Recently, imidazopyridines have emerged as a highly relevant class of compounds in medicinal chemistry and pharmaceutical research due to their remarkable versatility and therapeutic potential, including anticancer [9–17], antiprotozoal [18], antiviral [19], antimicrobial [20] and many other bioactivities [21–23].

In addition to traditional synthetic techniques, novel methods for synthesising derivatives with structural diversity at the 2- and 3-positions of the imidazopyridine moiety are being rapidly developed to capitalise on the growing interest in the properties and applications of imidazo[1,2-α]pyridines [24–29]. Approximately 5 % of the world's current medication supply can be produced through multicomponent reactions (MCRs) [24]. One variant of these MCRs is the GBB-3CR, which efficiently and economically synthesises imidazo[1,2-α]pyridines [30–32]. The GBB reaction involves the condensation of 2-aminoazines **1** with catalytically activated aldehydes and isocyanides in a one-pot, one-step process. Employing GBB-3CR for the synthesis of imidazo[1,2-α]pyridines has led to the development of several marketed drugs, such as alpidem two and saripidem **3** (Fig. 1A), as well as bioactive lead compounds (Fig. 1B).

Numerous studies have explored the bioactivity of imidazo[1,2-α]

* Corresponding authors.
E-mail addresses: s.raheem@westminster.ac.uk (S. Raheem), n.maharik@najah.edu (N. Al-Maharik).

https://doi.org/10.1016/j.molstruc.2025.142549
Received 27 March 2025; Accepted 30 April 2025
Available online 2 May 2025

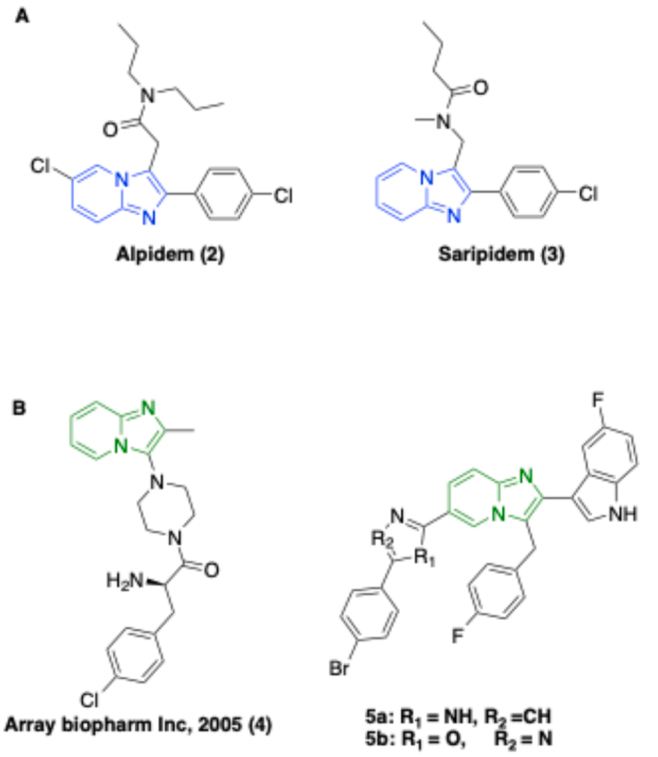

Fig. 1. A. Structures of alpidem **2** and saripidem **3** (24); B. anticancer lead compound **4** and antibacterial lead compounds **5a** and **5b** [20].

pyridines, showing potential antiproliferative effects against various cancer cell types. Garamvolgyi *et al.* effectively synthesised imidazo[1,2-α]pyridine derivatives that inhibited skin cancer cell proliferation with IC_{50} values lower than 0.04 μM [17]. Additionally, Buckmelter and colleagues described a new derivative of imidazo[1,2-α]pyrazine with an indanone oxime substituent that was particularly potent, with an IC_{50} in the nanomolar range [33].

Developing prospective novel anticancer drugs can reduce resistance to existing treatment. Based on these findings, we report the synthesis of novel derivatives of imidazo[1,2-α]pyridine and imidazo[1,2-α]pyrazine utilising GBB-3CR, as well as their *in vitro* efficacy as anticancer agents.

2. Results and discussion

2.1. Chemistry

2.1.1. Synthesis

Derivatives of imidazo[1,2-α]pyridine and imidazo[1,2-α]pyrazine were synthesised via an acid-catalysed GBB-3CR, as detailed in Scheme 1. The synthesis procedure involved a condensation reaction of 2-aminopyridine **1a** or 2-aminopyrazine **1b** with various aldehydes **6a-h**, using a small quantity of *p*-toluenesulfonic acid or scandium triflate as catalysts at 50 °C under a nitrogen atmosphere. This was followed by a nucleophilic attack of *p*-fluorophenyl isocyanide **7** and subsequent cyclisation of the resulting imide intermediate, yielding a series of 3-aminoimidazole[1,2-α]pyridines **8-14** and 3-aminoimidazo[1,2-α]pyrazines **15-20** in moderate yields (31.50 % - 61.70 %) (Fig. 2).

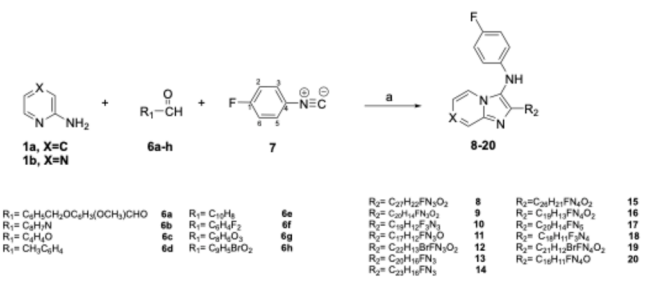

Scheme 1. Reagents and conditions: (**a**) *p*-TsA.H_2O or scandium triflate (Sc$(OTf)_3$), MeOH: CH_2CI_2 (1:1) or MeOH only, 1h, 50 °C.

The presence of electron-donating (ED) groups on the benzaldehydes, such as methoxy groups in compounds **8** and **15**, may have increased the yield, as these compounds exhibited the highest yield values among those synthesised (>40 %). The yield was higher than that obtained for compound **18**, which bore the electron-withdrawing (EW) difluorophenyl group. Additionally, a comparison between imidazopyridine **11** and its counterpart, imidazopyrazine **20**, revealed that the pyridine moiety yielded slightly more than the pyrazine moiety (39.8 % vs 35.9 %, respectively). However, in other cases, the opposite trend was observed when comparing compounds **8** and **15**. Imidazopyridine **8** was produced in a lower yield than its imidazopyrazine counterpart **15** (40.40 % vs 61.70 %, respectively). The modest yields of the products could also be attributed to the repeated use of flash chromatography and recrystallisation to obtain ultrapure compounds for biological screening.

The structures of the compounds **8-20** were determined using ^{1}H, ^{19}F, and ^{13}C-NMR and IR spectroscopy. For example, the IR analysis of 2-(benzo[d][1,3]dioxol-5-yl)-N-(4-fluoro-phenyl)imidazo[1,2-α]pyridin-3-amine (**9**) displayed major absorption bands at 1633 cm^{-1}, 1573 cm^{-1}, and 1342 cm^{-1}, corresponding to the stretching vibrations of C=N, C=C, and C-N bonds, respectively. Additionally, a band was observed at 3215 cm^{-1}, which was assigned to the N-H stretching of compound **9**. All compounds showed a strong absorption band related to aromatic C=C stretching, ranging from 1449 to 1514 cm^{-1}. The characteristic bands for C=N, C=C, and C-N stretching for most products were found in the 1572 – 1633 cm^{-1}, 1522 – 1599 cm^{-1}, and 1323 – 1360 cm^{-1}, respectively. The ^{1}H NMR spectrum of the compound showed proton resonances at 6.52 – 7.81 ppm, attributable to the aromatic, pyridine, phenyl and benzene rings. A single resonance for the NH group appeared at 5.51 ppm, corresponding to the *p*-fluorophenyl amine. A singlet signal to the protons of the 1,3-dioxole group appeared at 5.96 ppm.

2.1.2. Crystal structure description

The X-ray structure analysis of the imidazopyrazine derivatives proved the structure elucidation obtained from the spectral characterisation. For **9**, the compound formula is $C_{20}H_{14}N_3O_2F$, where the structural parameters (bond distances and angles) are listed in Table 1. As shown in Fig. 3A, the benzodioxolyl and fluorophenyl moieties are not planar with the imidazopyrazine moiety, where the twist angles are 3.48 and 87.59°, respectively. The twist angle of the fluorophenyl group is high, possibly due to the bulky character of the neighbouring benzodioxolyl moiety. The twist angles (e.g. 87.59° in compound **9** vs 75.65° in compound **20**) influence molecular planarity and electronic delocalisation, impacting lipophilicity, solubility, and bioavailability. A lower twist angle (more planar structure) can enhance π-electron delocalisation, which may improve target binding through π-stacking interactions with aromatic residues in biological macromolecules [34,35]. Similarly, π-π stacking distances (C…C: 3.20 – 3.39 Å) suggest varying degrees of intermolecular interactions in the solid state, which could influence compound solubility and aggregation in solution.

The packing of **9** is controlled by strong N19-H19···N1 hydrogen bond where the H19···N1 and N19···N1 distances are 2.15(2) and 3.05(17) Å, respectively (Fig. 3B and C). This interaction is crucial in stabilising the crystal lattice by reinforcing intermolecular connectivity. The strength and directionality of hydrogen bonding can significantly influence molecular organisation, potentially impacting solubility and dissolution rates in a biological environment [36,37]. Strong hydrogen bonding interactions, as observed in compound **9**, may reduce solubility due to tighter molecular packing, which can affect the compound's bioavailability and pharmacokinetics [38].

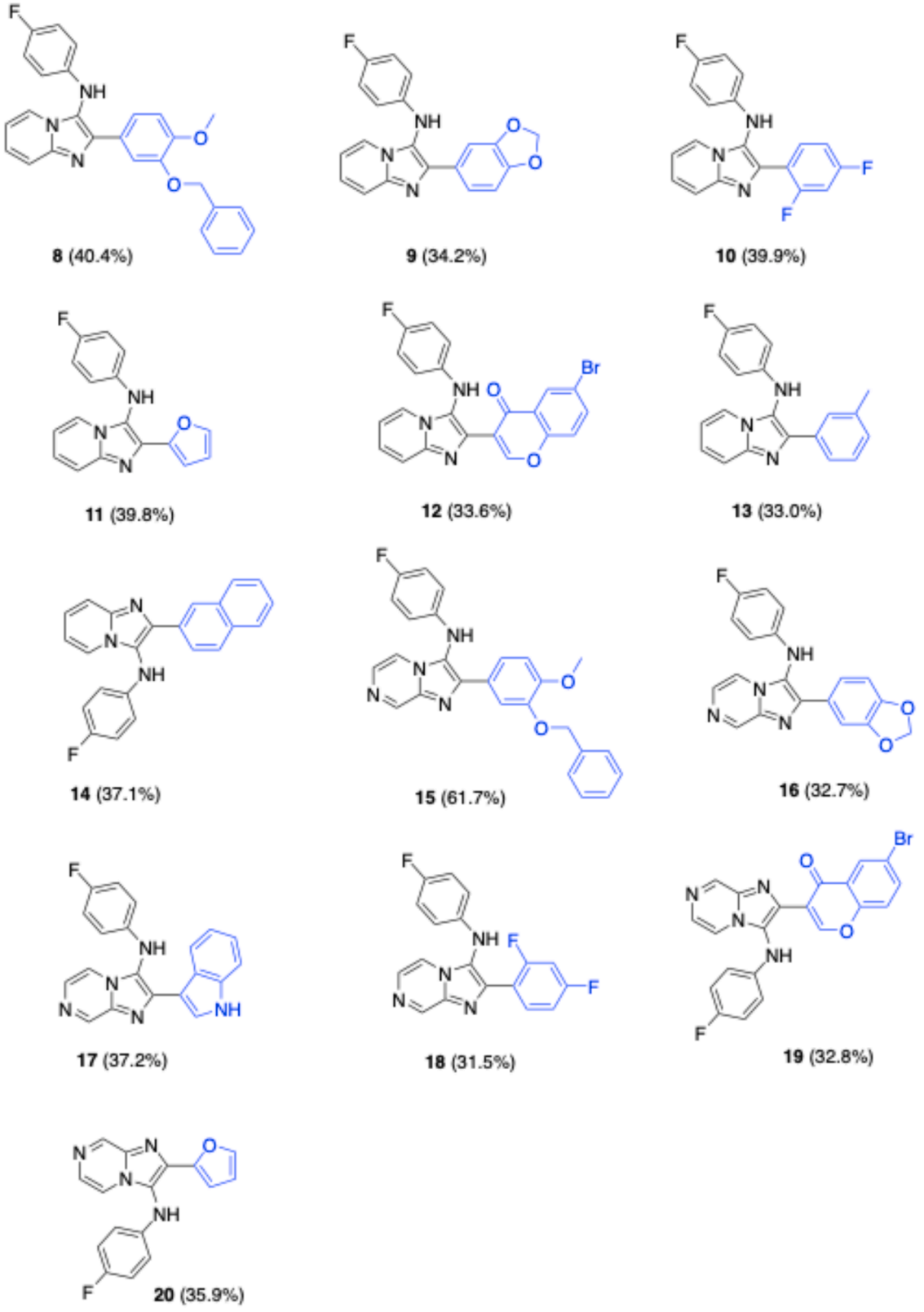

Fig. 2. Structure-activity relationships of the synthesised compounds **8-20**.

For **20,** the compound formula is $C_{16}H_{13}FN_4O_2$, and the target compound $C_{16}H_{11}FN_4O$ is crystallised with one water molecule. The structural parameters (bond distances and angles) are listed in Table 1. As shown in Fig. 4A, the planar imidazopyrazine moiety is connected by fluorophenyl and furanyl moieties, which are also not perfectly coplanar with the former aromatic ring systems. The furanyl moiety is slightly twisted from the imidazopyrazine plane by 5.61°. In contrast, the fluorophenyl group is strongly twisted by 75.65° but less than that in **9** due to the little bulky character of the neighbouring furanyl moiety.

The crystal water molecule plays an essential role in the molecular

Table 1
Bond lengths (Å) and angles (°) for **9** and **20**.

Bond	Length/Å	Bond	Length/Å
Cpd 9	**Cpd 9**	**Cpd 20**	**Cpd 20**
F23-C23	1.37(19)	F19-C19	1.37(14)
O13-C12	1.38(2)	O14-C10	1.37(14)
O13-C14	1.44(2)	O14-C13	1.37(16)
O15-C14	1.44(2)	N15-C16	1.40(15)
O15-C16	1.38(19)	N4-C9	1.38(15)
Bond	**Angle/°**	**Bond**	**Angle/°**
C12-O13-C14	105.10(13)	C13-O14-C10	106.12(10)
C16-O15-C14	105.32(13)	C3-N15-C16	122.57(10)
C9-N1-C2	105.60(14)	C3-N4-C9	107.30(9)
C5-N4-C3	129.87(15)	C5-N4-C3	131.54(10)
C5-N4-C9	123.17(15)	C5-N4-C9	121.15(10)

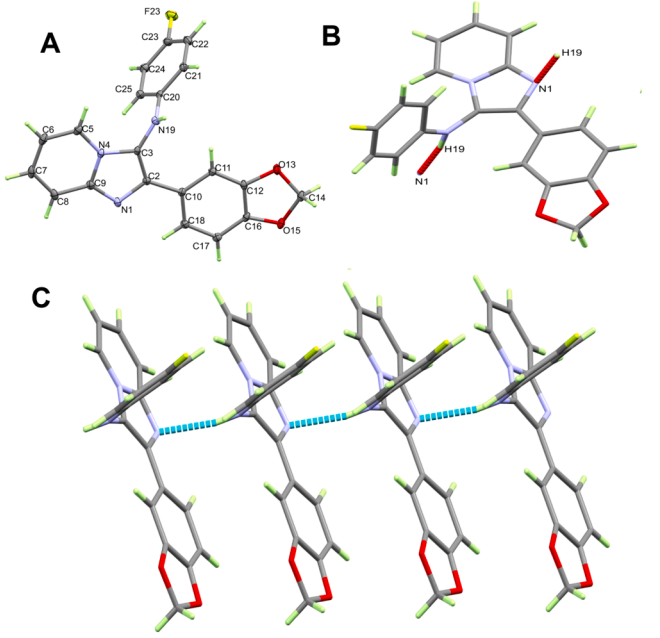

Fig. 3. Structure with atom numbering for **9 (A)**, essential contacts **(B)** and packing view **(C)**.

packing **20**. It forms four crucial hydrogen bonds with the organic molecule where this solvent molecule works as both hydrogen bond donor and acceptor (Fig. 4B). The O21-H21A and O21-H21B as hydrogen bond donor groups form with N1 and N7 the strong hydrogen bonds with Hacceptor distances of 2.00(17) and 1.92(17) Å, respectively while the respective O···N distances are 2.94(13) and 2.84(14) Å. In addition, there is another significant hydrogen bond occurred between the N15-H15 and the crystal water O21 atom as hydrogen bond acceptor where the H15···O21 and N15···O21 distances are 1.96(14) and 2.86(13) Å, respectively (Table 2). Another extended interaction occurred with the crystal water molecule, C18-H18···O21, where the C18···O21 distance is 3.25(16) Å. The presentation of a packing view for **20** is shown in Fig. 4C.

In addition, both compounds showed the presence of π-π stacking interactions, as seen in Fig. 5. These interactions may contribute to enhanced stabilisation with protein binding sites, influencing molecular binding affinity, cellular uptake, and bioavailability [39]. The significant π-π contacts in compound **9** (C7···C11 (3.39(2) Å), C7···C12 (3.20(3) Å) and C8···C16 (3.27(2) Å) compared to compound 20 (C8···C10 = 3.39 Å) suggests a potential role in differential biological activities.

2.1.2.1. Hirshfeld surface analysis. Hirshfeld surface analysis helps detect all intermolecular interactions in the crystal structure. Even weak

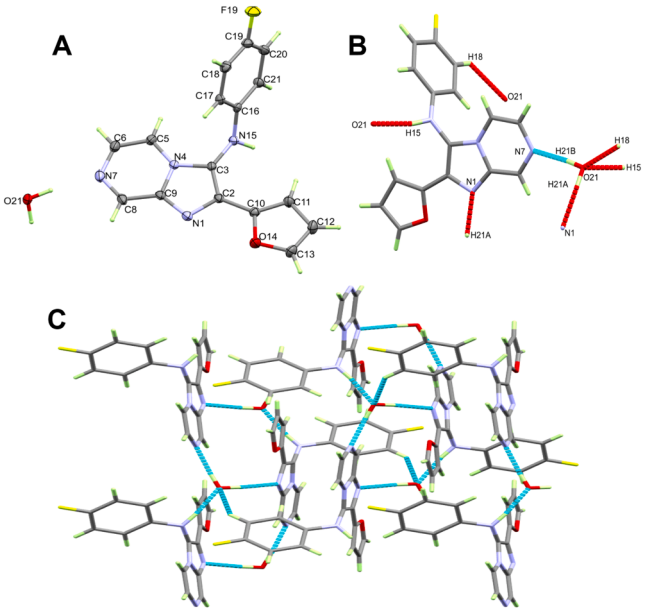

Fig. 4. Structure with atom numbering for **20 (A)**, essential contacts **(B)** and packing view **(C)**.

Table 2
Hydrogen bonds for **9** and **20** [Å and °].

D-H...A	d(D-H)	d(H...A)	d(D...A)	<(DHA)	Symm. Code
9					
N19-H19...N1	0.91(2)	2.15(2)	3.05 (17)	169.00(2)	1+x,y,z
20					
N15-H15... O21	0.91 (14)	1.96 (14)	2.86 (13)	169.20 (15)	x,-1+y,z
O21-H21A... N1	0.95 (16)	2.00 (17)	2.94 (13)	169.40 (16)	1-x,1/2+y,3/ 2-z
O21-H21B... N7	0.93 (17)	1.92 (17)	2.84 (14)	174.90 (15)	
C18-H18... O21	0.95	2.50	3.25 (16)	135.00	x,3/2-y,-1/2+z

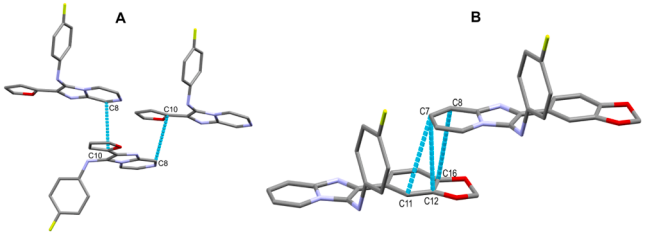

Fig. 5. The π-π stacking interactions in **20** (A) and **9** (**B**).

forces with small contributions in the molecular packing could be analysed using this tool. In the studied crystal structures, all possible intermolecular forces that control the crystal stability are listed in Fig. 6. The primary contributing contacts for both compounds are the H···H and H···C interactions. Their percentages in compound **9** are 36.7 and 28.5 %, respectively, while in the case of **20**, the corresponding values are 37.1 and 22.0 %. Other less contributing intermolecular contacts were detected, such as O···H (11.50 %), N···H (6.70 %) and F···H (7.0 %) in **9**. These interactions contributed to the molecular packing **20** by 5.60, 9.30 and 11.01 %, respectively.

The d_{norm} Hirshfeld map helps detect the short meaningful interaction that appeared as red spots on this map. For compound **9**, many short

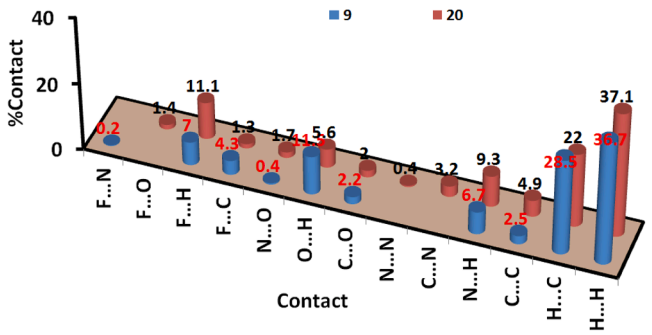

Fig. 6. The percentage of contacts is **9** and **20**.

contacts were detected: the O···H, N···H, C···H, C···C, F···C and H···H. For clarity, the regions shared in these intermolecular contacts are labelled by letters **A-F** in the overall d_{norm} map shown in Fig. 7. In the exact figure, their fingerprint plots are presented. The presence of symmetrical wings or spikes in the fingerprint plots of all these contacts revealed that the surface acts as a donor and acceptor for these interactions to the same extent. In addition, the shape index map contains the red/blue triangles, characteristic of the presence of π-π stacking. The region from the molecular surface that contributed to this interaction is surrounded by a black rectangle for more clarity (Fig. 7).

For compound **20**, there are four short significant contacts: the O···H, N···H, C···H and C···C, which all appeared as red spots in the d_{norm} map. Their fingerprint plots presented in Fig. 8 leave no doubt about the role of the molecular surface in the O···H and N···H hydrogen bonds. The surface acts as a better hydrogen bond acceptor regarding the N···H contacts rather than being a hydrogen bond donor, as indicated by the

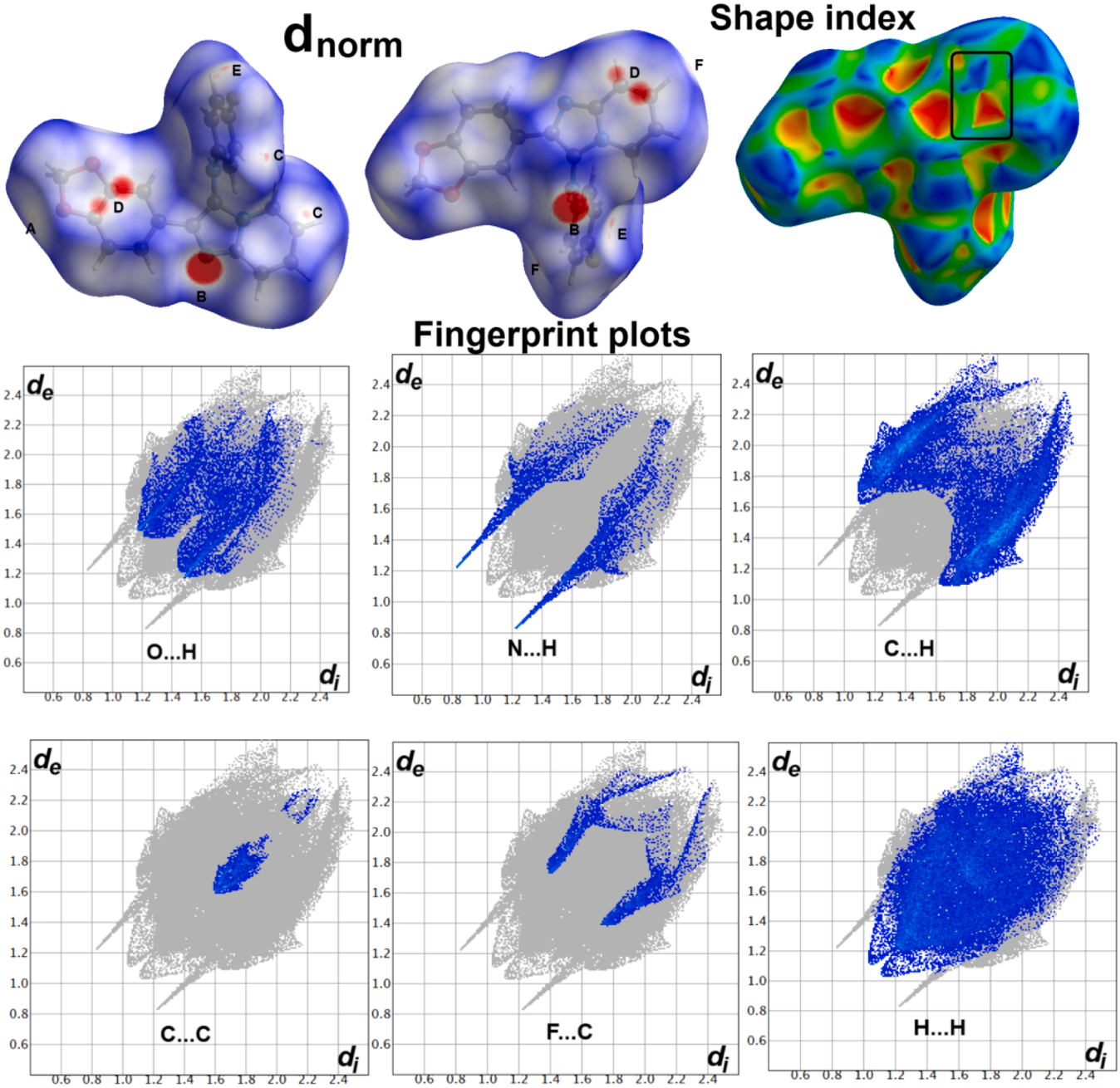

Fig. 7. Hirshfeld analysis of **9**; O···H (A), N···H (B), C···H (C), C···C (D); F···C (E) and H···H (F).

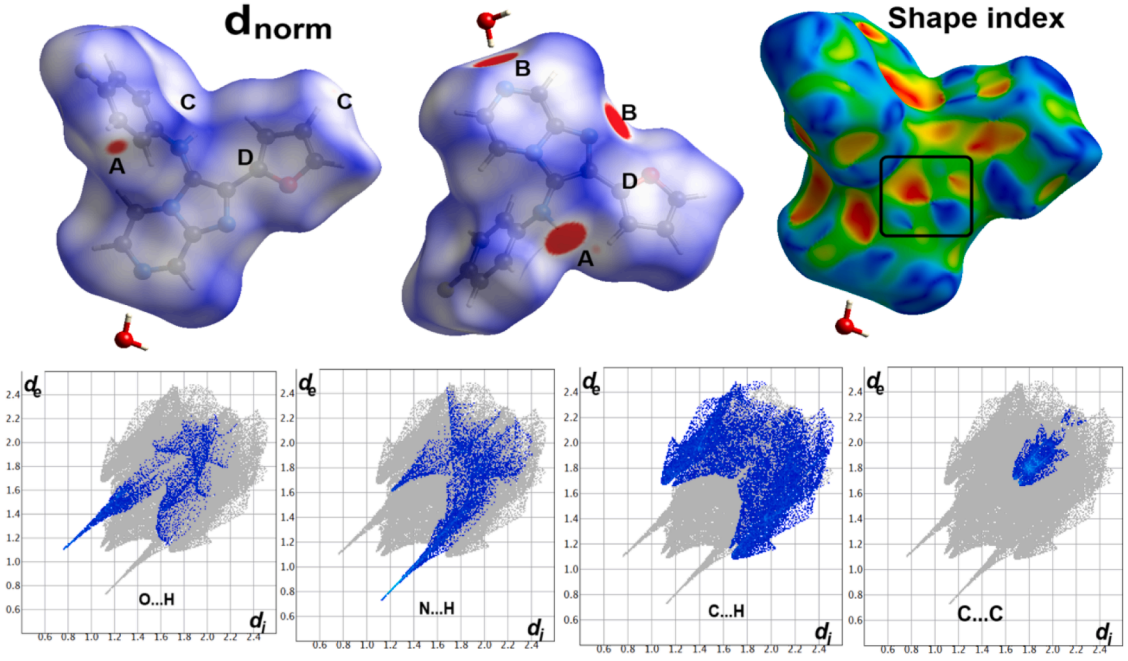

Fig. 8. Hirshfeld analysis of **20**; O···H (A), N···H (B), C···H (C) and C···C (D).

sharp spike at the right part of the corresponding fingerprint plot. In contrast, the surface is more likely to be a hydrogen bond donor concerning the O···H contact rather than a hydrogen bond acceptor, as indicated by the sharp spike at the left part of the corresponding fingerprint plot. Regarding C···H contacts, the two wings are almost symmetrical, indicating that the surface acts as both hydrogen bond donor and acceptor to similar extents. In this case, no red spots were detected for the C···C contacts, although red/blue triangles were present in the shape index map. Hence, the π-π stacking is weaker in compound **20** compared to **9**.

While Hirshfeld surface analysis offers valuable insights into crystal packing and intermolecular interactions, its direct correction with biological performance remains uncertain [40]. Further studies, incorporating solubility measurements, protein-ligand binding assays, and in vitro pharmacokinetic evaluations, are required to establish a more comprehensive relationship between solid-state molecular organisation and biological activity.

2.1.2.2. Molecular orbitals (HOMO-LUMO). DFT calculations were performed on five molecules to examine their electronic structure and determine the corresponding HOMO-LUMO gap. The five molecules are **15, 16, 17, 18** and **19**. Fig. 9 shows the HOMO and LUMO surface plots for all five compounds. In the plots, red indicates a positive sign of the wave function, while green represents a negative sign. The HOMO

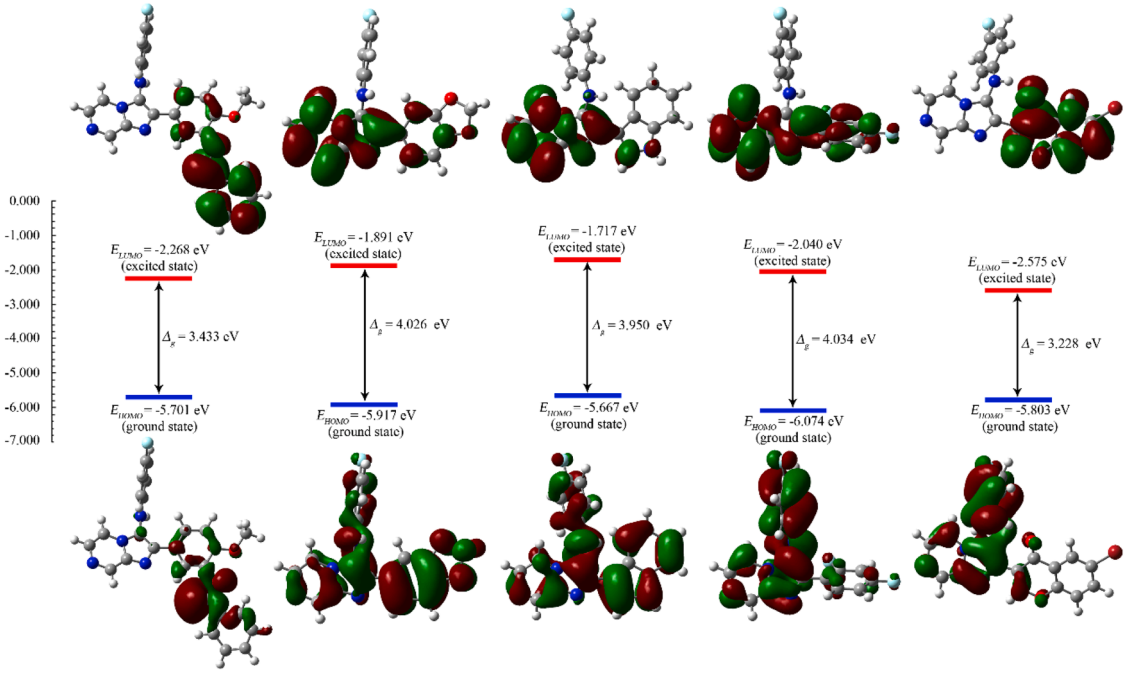

Fig 9. Molecular orbitals' surface plots of compounds **15, 16, 17, 18** and **19**.

surface of compound **15,** as shown in Fig. 9, is localised over the aromatic substituent (benzyloxy-methoxyphenyl). In contrast, for compound **16** and compound **17**, the HOMO is distributed throughout the entire molecule, indicating an admixture of orbitals from most atoms in the structure. On the other hand, the HOMO for compounds **18** and **19** is more localised in a smaller region, primarily over the 4-fluorophenyl and imidazo[1,2-α]pyrazine moieties with a little extension towards the aromatic substituent.

The LUMO for all molecules is more localised over a small region. For the LUMO, the 4-fluorophenyl group does not contribute to its formation. Similar to HOMO, the LUMO surface of compound **15** is also localised over the benzyloxy-methoxyphenyl region. The LUMO for compounds **16**, **17**, and **18** are primarily localised on the imidazo[1,2-α] pyrazine core and other electron-withdrawing molecule regions. For compound **19,** the LUMO is exclusively localised to the aromatic regions. The 4-fluorophenyl group does not contribute to the LUMO formation, suggesting a different electronic distribution compared to compounds **16, 17**, and **18**. The DFT calculated HOMO and LUMO energies are shown in Fig. 9. Compound **18** has the lowest HOMO energy, which is -6.074 eV. This is because compound **18** with difluorophenyl substituent introduces more electron-withdrawing groups, which lower the HOMO energy. The HOMO-LUMO gaps were calculated to be 3.43, 4.02, 3.95, 4.03, and 3.23 eV, respectively, for molecules **15, 16, 17, 18**, and **19**. The HOMO-LUMO gaps for molecules **15** and **19** are significantly smaller than that of molecules **16** and **18.** Compounds **16** and **18** are the two most potent in terms of inhibitory activity against cancer cells. These two molecules also have the largest HOMO-LUMO gap compared to the other three molecules. A large HOMO-LUMO gap signifies that the molecules are more stable as it requires more energy to excite an electron from HOMO [41]. It also indicates that they are more stable because a large HOMO-LUMO gap leads to low electron affinity; therefore, they have a poor ability to obtain electrons. A larger HOMO-LUMO gap is also associated with smaller reducibility [42].

The large HOMO-LUMO gap does not necessarily correlate with reduced biological activity. Instead, the distribution of molecular orbitals suggests that compounds **16** and **18** maintain key interactions with biological targets despite their electronic stability. Despite their large HOMO-LUMO gap, compounds **16** and **18** exhibit significant inhibitory activity against cancer cells.

2.2. Biology

2.2.1. Anticancer activity

Since several studies reported the imidazopyridines and imidazopyrazines as promising anticancer agents [9–17], the cytotoxicity of the synthesised imidazo[1,2-α]pyridine/pyrazine compounds **8-20** was evaluated against breast (MCF-7), colon (HT-29), and melanoma (B16F10) cancer cell lines, as well as a normal cell line (MEF). The results are shown in Table 3 and Fig. 10.

As shown in Table 3, the imidazopyrazine compound **18**, bearing a 2,4-difluorophenyl moiety (electron-withdrawing group) at the C-2 position and a *p*-fluorophenyl amine at the C-3 position, exhibited the highest inhibitory activity against MCF-7, with an IC_{50} of 9.60 ± 3.09 μM compared to the other tested compounds. Compound **18** showed significant anticancer activity against HT-29 (IC_{50}= 22.61 ± 0.18 μM) but weak activity against B16F10 (IC_{50} = 150.29 ± 0.10 μM). In contrast, the imidazopyridine counterpart **10** showed notable activity only against BF16F10 (IC_{50} = 47.50 ± 12.52 μM). This indicates that the combination of imidazopyrazine with *p*-fluorophenyl at the C-3 position, as exemplified by compound **18**, is crucial for maintaining anticancer activity when the 2,4-difluorophenyl moiety is present at the C-2 position. This may be attributed to extra nitrogen in the pyrazine ring, which contributes to additional hydrogen bonding in the target pocket, enhancing interaction stability. Moreover, compound **18** contains three halogen atoms (F) on phenyl rings, which enhances its effectiveness. In drug development, the insertion of halogen atoms into a lead drug candidate often produces more lipophilic analogues and less water soluble. As a result, halogen atoms are utilised to increase penetration across lipid membranes and tissues [34].

Table 3
Cytotoxic activities of the synthesised compounds (**8-20**) against the MCF-7, HT-29, B16F10 and MEF cell lines.

Cpd's Designation	[a]IC_{50} (μM)			
	MCF-7	HT-29	B16F10	MEF
Paclitaxel (Taxol)	0.01	0.02	55.70	17.23
8	> 200.00	> 200.00	190.59 ± 17.47	> 200.00
9	> 200.00	171.68 ± 4.19	53.37 ± 0.16	> 200.00
10	> 200.00	> 200.00	47.50 ± 12.52	> 200.00
11	> 200.00	> 200.00	> 200.00	> 200.00
12	116.13 ± 0.59	107.26 ± 1.43	65.45 ± 0.85	68.62 ± 5.45
13	> 200.00	> 200.00	> 200.00	> 200.00
14	> 200.00	96.12 + 7.76	96.26 ± 4.46	> 200.00
15	> 200.00	> 200.00	> 200.00	> 200.00
16	47.28 ± 14.23	12.98 ± 0.40	27.45 ± 1.26	165.75 ± 5.52
17	> 200.00	> 200.00	171.41 ± 2.00	> 200.00
18	9.60 ± 3.09	22.61 ± 0.18	150.29 ± 0.10	67.09 ± 0.59
19	32.71 + 3.17	112.26 ± 0.44	108.06 ± 2.23	177.21 ± 2.50
20	> 200.00	66.44 ± 28.31	> 200.00	> 200.00

[a] The IC_{50} values (μM) represent an average of two independent experiments (mean ± SD).

Compounds **9** and **16**, containing the piperonal moiety, exhibited similar behaviour. Imidazopyridine **9** showed no bioactivity against MCF-7. However, the simultaneous inclusion of *p*-fluorophenyl amine as the C-3 position and pyrazine moieties restored bioactivity against MCF-7, as demonstrated by compound **16** with an IC_{50} of 47.28 ± 14.23 μM. Compound **16** also exhibited excellent anticancer activity against HT-29 (IC_{50} = 12.98 ± 0.40 μM) and B16F10 (IC_{50} = 27.45 ± 1.26 μM). Conversely, compound **9** displayed weak activity against HT-29 (IC_{50} = 171.68 ± 4.19 μM) and good activity against B16F10 (IC_{50} = 53.37 ± 0.16 μM).

In congruence, Ren et al. [34] synthesised a GBB compound similar to compound **16**, imidazopyrazine with piperonal moiety at C-2, based on the observation of ATP-competitive heat shock protein 90 (Hsp90) inhibitors bearing the 8,9-disubstituted adenine motif, which could be replaced by the 2,3-disubstituted 8-aminoimidazo[1,2-*a*]pyrazine scaffold. The compound demonstrated several contacts with the ATP binding site, including hydrogen bonding, π-stacking, and van der Waals interactions, making it a good candidate as a cytotoxic agent [43].

Compounds **11** and **20** both feature a furan moiety at the C-2 position. The imidazopyridine compound **11** showed no anticancer activity against MCF-7, HT-29, or B16F10 cancer cell lines. In contrast, the imidazopyrazine compound **20** exhibited no activity against MCF-7 and B16F10 but showed good activity against HT-29 (IC_{50} = 66.44 ± 28.31 μM). The bromo-substituted chromone moiety at the C-2 position of compounds **12** and **19** may contribute to their biological activity against B16F10 and MCF-7 cancer cell lines (IC_{50} = 65.45 ± 0.85 μM and 32.71 ± 3.17 μM, respectively). Compound **19**, containing the pyrazine moiety, could be more potent than compound **12**, which has a pyridine moiety. Compound **12** also showed weak activity against HT-29 (IC_{50} = 107.26 ± 1.43 μM) and MCF-7 (IC_{50} = 116.13 ± 0.59 μM), while compound **19** exhibited weak anticancer activity against both HT-29 (IC_{50} = 112.26 ± 0.44 μM) and B16F10 (IC_{50} = 108.06 ± 2.23 μM).

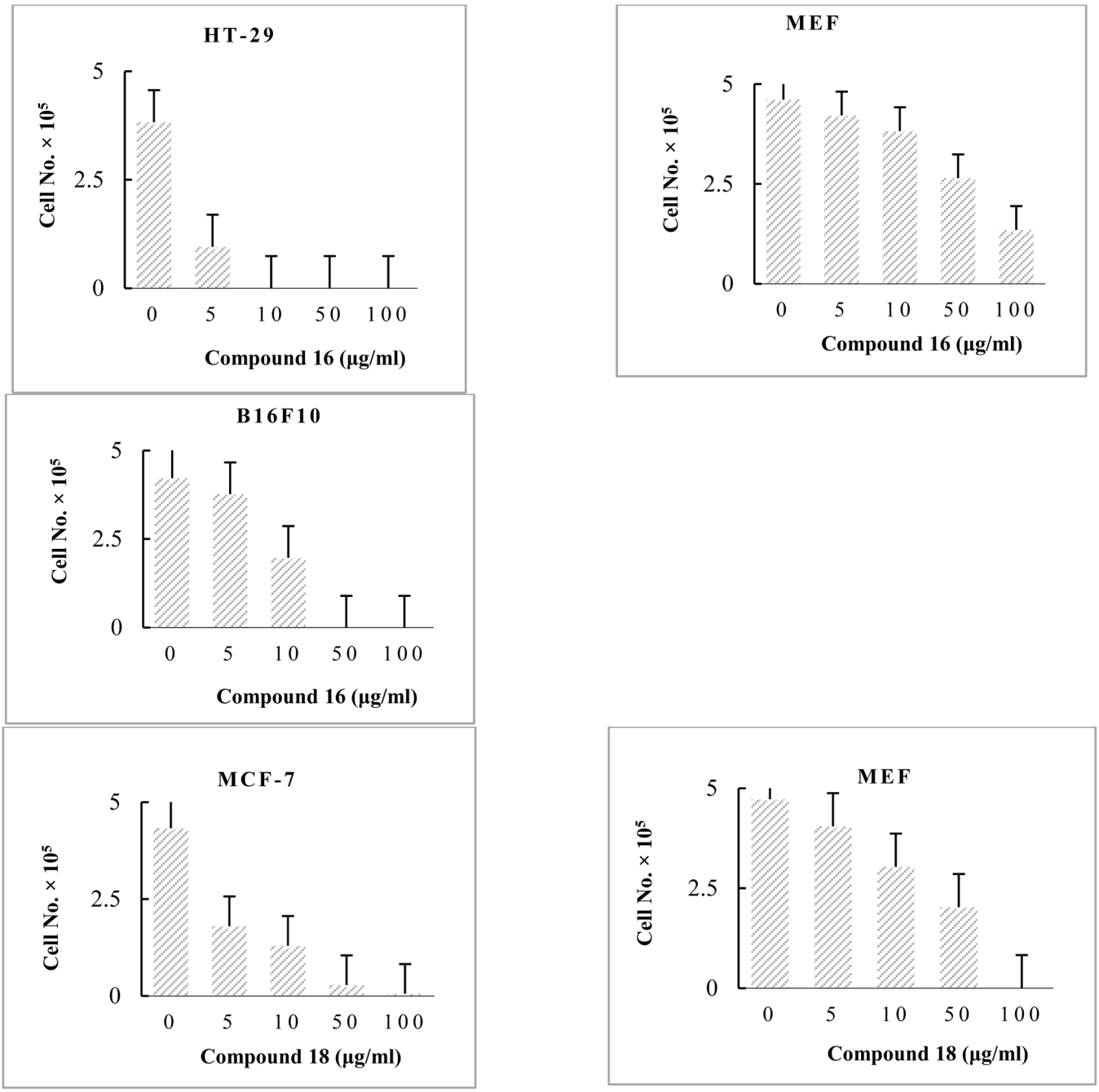

Fig. 10. Histograms of the bioactivity of the most potent compounds against various cancer cell types, as well as against the normal MEF cells.

Furthermore, some analogues showed weak to no bioactivity against some or all cancer lines. For example, compound **14**, which contains a naphthalene moiety at the C-2 position, was ineffective against MCF-7 and had weak activity against HT-29 and B16F10 (IC_{50} = 96.12 ± 7.76 and 96.26 ± 4.46 µM). Additionally, compound **17**, with an indole moiety at the C-2 position, was not bioactive against MCF-7 and HT-29 but exhibited weak anticancer activity against BF16F10 (IC_{50} = 171.41 ± 2.00 µM). Compounds **8, 13**, and **15** showed no bioactivity against cancer cell lines.

Considering both effectiveness and safety, compound **16** is a promising lead compound as an anticancer agent against both HT-29 (IC_{50} = 12.98 ± 0.40 µM) and B16F10 (IC_{50} = 27.54 ± 1.26 µM), with an IC_{50} against normal cells (IC_{50} = 165.75 ± 5.52 µM), representing approximately thirteen times and six times the IC_{50} values against both cancer cell lines, respectively. Compound **18** can also be considered a potent anticancer lead compound due to its high toxicity against MCF-7 (IC_{50} = 9.60 ± 3.90 µM), which is about seven times lower than its cytotoxicity against MEF (IC_{50} = 67.09 ± 0.59 µM). These IC_{50} values confirm the high selectivity of the two promising compounds (**16** and **18**) for cancer cells over normal cells, as shown in the histograms in Fig. 10.

Many hypotheses can explain the mechanism of action for the anticancer activity of imidazopyridines. For example, phosphatidylinositol 3-kinase (PI3K) protein kinases represent one target in cancer progression. PI3Ks transduce signals from numerous growth factors and cytokines by producing phospholipids, activating the kinases AKT and mTOR and other downstream effector pathways that control the cell cycle via intracellular signalling pathways [44]. Dysregulated activation of the PI3K/AKT/mTOR pathway causes significant cell growth and survival disruptions, resulting in angiogenesis, metastatic competence, and therapy resistance in many cancer types. Imidazopyridines have

demonstrated potential inhibitory activity against protein kinases. Imidazo [1,2-*a*]pyridines are among several PI3K hinge region binders. This scaffold is essential because it resembles the adenine ring of ATP and stabilises the enzyme's binding site by creating hydrogen bonds with a valine residue in this area. Furthermore, C-2 or C-3 functionalisation of imidazo[1,2-*a*]pyridine improves access to PI3K's ribose binding pocket. The remarkable capacity of imidazopyridine scaffolds to create several critical interactions, including hydrogen bonds inside kinases' hinge regions, demonstrates their potential for precise target engagement [44].

Compared to the control (untreated cancer cells), morphological changes in the three cancer cell lines (MCF-7, HT-29, and B16F10) were investigated after treatment with the most potent and safe compounds, **16** and **18**. As shown in the photographs, all treated cells lost their original forms. Their severe shrinkage suggests the investigated compounds exhibited strong anticancer properties, particularly at higher doses (Fig. 11).

2.2.2. *Structure-activity relationship (SAR) analysis*

In this work, we observed that the biological activity of the tested compounds varied inconsistently across different cancer cell lines, preventing the establishment of a robust quantitative SAR model. While lipophilicity (LogP) may contribute to activity, its influence appears minimal in this dataset. Instead, activity is primarily governed by the specific molecular fingerprint of each compound, suggesting that subtle structural variations play a dominant role in their bioactivity. Given the relatively small library of compounds analysed, statistical correlations necessary for a reliable QSAR model are difficult to establish, as a limited dataset increases the likelihood of overfitting or weak predictive power.

Given these limitations, a qualitative structure-activity relationship approach is more suitable for this study. Rather than relying on statistical modelling, qualitative SAR allows us to analyse key structural features and functional groups contributing to bioactivity trends. [1,2-α] pyrazine and pyridine central core are essential for displaying the anticancer properties [45]. The key structural modifications of these analogues are only at the C-2 position, where the differences between electron-withdrawing and electron-donating groups greatly impact the resulting anticancer activity in different cancer cells. Compound **18,** which features a 2,4-difluorophenyl moiety at C-2 and *p*-fluorophenyl amine at C-3, exhibited the highest activity against MCF-7 (IC_{50} = 9.60 ± 3.09 μM).

In contrast, compound **10**, the imidazopyridine analogue of **18**, showed significantly lower activity against B16F10 (IC_{50} = 47.50 ± 12.52 μM). This highlights the potential contribution of the additional nitrogen in the pyrazine core to enhanced bioactivity. The presence of multiple fluorine atoms in compound **18** may have improved lipophilicity, cellular permeability and target binding affinity (Fig. 12).

The incorporation of the piperonal moiety at C-2 in compound **16** conferred dual anticancer activity against HT-29 (IC_{50} = 12.98 ± 0.40 μM) and B16F10 (IC_{50} = 27.45 ± 1.26 μM), suggesting that further exploration of this motif could be valuable. However, its imidazopyridine analogue **9** showed weaker activity, particularly against MCF-7 and HT-29. This indicates that the combination of pyrazine and piperonal enhances interactions with cancer targets, possibly due to additional hydrogen bonding sites [46]. The furan-substituted compound **11** was inactive, while its pyrazine counterpart, compound **20,** exhibited moderate activity against HT-29 (IC_{50} = 66.40 ± 28.31 μM). This suggests that furan substitution alone may not be sufficient for strong anticancer activity unless paired with a favourable core scaffold—the bromo-substituted chromone moiety in compounds **12** and **19** conferred selectivity towards different cancer lines. Compound **19** showed good activity against MCF-7 (IC_{50} = 32.71 ± 3.17 μM), while compound **12** was more active against B16F10 (IC_{50} = 65.45 ± 0.85 μM).

2.2.3. *ADMET predictions*

The in silico ADMET properties provide valuable insights into why certain compounds exhibit varying cytotoxicity across cancer cell lines. By integrating these predictions with the IC_{50} values, we can identify potential factors influencing bioactivity. Most compounds exhibit high intestinal absorption (>80 %), suggesting good bioavailability. However, compounds **8, 9, 10, 11, 13**, and **15** show weak cytotoxicity (IC_{50} > 200 μM) in most cell lines, indicating that absorption alone is not a key determinant of anticancer activity. Compounds with poor BBB permeability (compound **8**) may have limited intracellular access, potentially explaining the lack of activity in B16F10 (melanoma) and other cell lines. Compounds **12, 16**, and **18** showed moderate BBB permeability and exhibited higher cytotoxicity (IC_{50} < 100 μM) in at least one cell

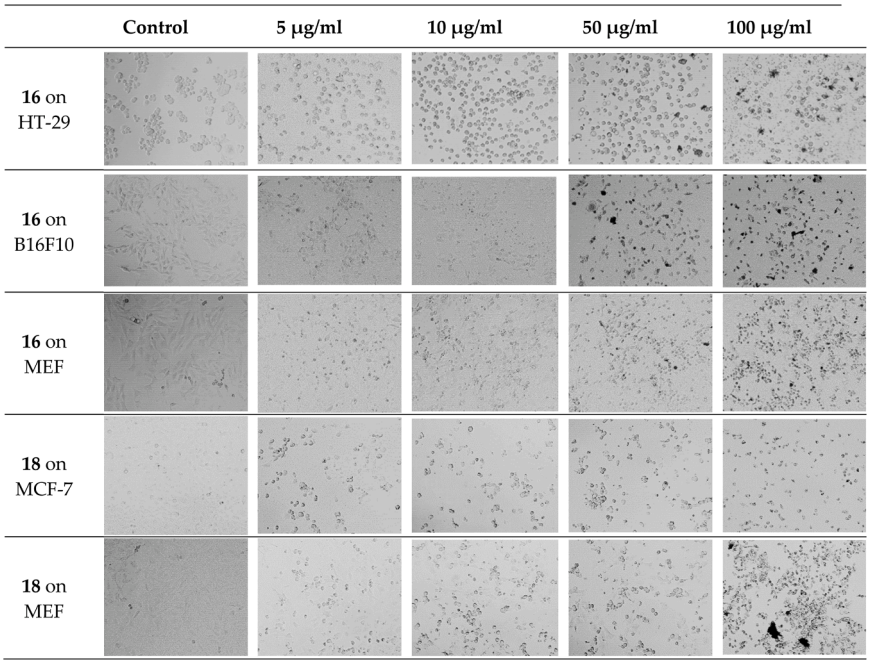

Fig. 11. Morphological changes in cancer and normal cell lines treated with the most potent compounds and in the control (untreated cancer cells).

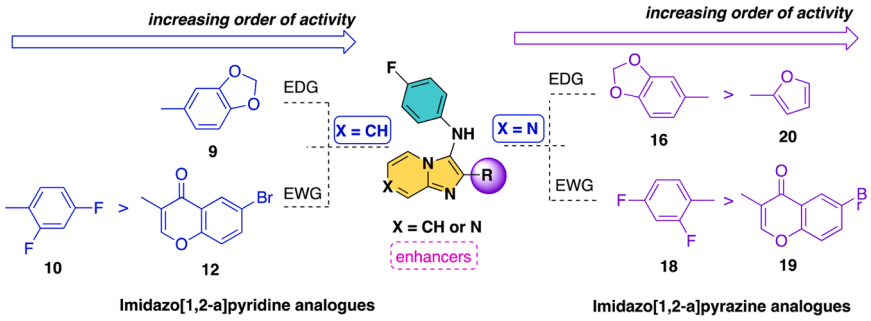

Fig. 12. Structure-activity relationship of Imidazo[1,2-a]pyridine/pyrazine analogues.

line, suggesting their better ability to penetrate and interact with intracellular targets. Hence, BBB permeability and CNS penetration variations may indicate differences in central nervous system accessibility, potentially affecting compounds' ability to engage intracellular targets. The total clearance varies, suggesting differences in metabolic stability and elimination rates. Compounds with higher clearance (compounds **13** and **17**) may have reduced intracellular retention, leading to lower bioactivity in cancer cells. Compounds with high absorption but rapid clearance may exhibit transient activity, while those with moderate clearance may have prolonged intracellular retention, enhancing cytotoxic effects [47].

AMES toxicity and hepatotoxicity in some compounds demonstrate cell line-specific activity depending on metabolic enzyme expression and detoxification mechanisms. The maximum tolerated dose fluctuates, which may correlate with variations in cytotoxicity across different cell lines. The PAINS (Pan-Assay Interference Compounds) alert is minimal (only compound **11**), suggesting that most compounds do not suffer from promiscuous binding, reinforcing the notion that specific molecular fingerprints primarily govern activity. Given these findings in Table 4, ADMET profiling helps rationalise why some compounds are more potent in particular cancer cell lines while others exhibit inconsistent activity. Future optimisation efforts should balance absorption, clearance, and toxicity profiles to enhance efficacy while minimising off-target effects.

3. Conclusions

The current study details synthesising a series of imidazo[1,2-α] pyridine/pyrazine derivatives (**8-20**) using acid-catalyzed GBB-3CR. The cytotoxic activity of all synthesised analogues against the cancer cell lines MCF-7, HT-29, and B16F10, as well as the normal MEF cell line, was evaluated using the Trypan blue exclusion test. Analysis of the most promising synthesised compounds, based on their potent inhibitory activity and selectivity for cancer cells over normal cells, revealed that imidazopyrazine **16**, featuring a piperonal moiety, could be an effective anticancer agent against both HT-29 and B16F10 cancer lines. Furthermore, compound **18** demonstrated promising anticancer activity against the MCF-7 cell line. Further research into these derivatives may yield more effective compounds that could serve as potent candidates for developing new anticancer medicines. X-ray structures for compounds **9** and **20** are presented for the first time. Their 3D molecular features and supramolecular packing are analysed using Hirshfeld analysis. Both compounds showed some π-π stacking interactions, which are more important in **9** than **20**. The dominant intermolecular interactions are the H···H and H···C contacts. Their high contribution in compound **9** (36.70 % and 28.50 %, respectively) may reduce solubility by increasing molecular rigidity.

In contrast, compound **20** (37.01 % and 22.0 %) may benefit from improved solubility and distribution due to its lower molecular packing density. DFT calculations provided insights into the electronic properties of selected compounds, revealing that a larger HOMO-LUMO gap correlates with enhanced stability, while molecular orbital distribution influences key biological interactions. Structure-activity relationship (SAR) analysis highlighted the critical role of C-3 substitutions, particularly the presence of electron-withdrawing groups and pyrazine cores, in modulating anticancer potency. ADMET predictions complemented experimental findings by rationalising variations in bioactivity through absorption, clearance, and toxicity profiles.

4. Experimental section

4.1. Chemistry

4.1.1. General information

The chemical compounds and solvents purchased from Sigma-Aldrich were utilised without further purification. The *p*-fluorophenyl isocyanide was synthesised using the methodology described by Weber and Gokel (1972) [30]. HPLC-grade methanol (MeOH) was acquired from Sigma-Aldrich and used for synthesis reactions under inert gas (N_2) conditions. ^{1}H-, ^{19}F-, and ^{13}C-NMR were recorded in $CDCl_3$ on 500 MHz Bruker AV III spectrometer. Chemical shifts are represented by the δ value (ppm), whereas coupling constants (*J*) are expressed in Hertz (Hz). CHN analyses were performed using Flash 2000 FT-IR spectra and were recorded using a Thermo Scientific Nicolet 1s5-Id3 Fourier transform infrared spectrophotometer. The progress of reactions was monitored using aluminum-supported Thin Layer Chromatography (TLC) silica gel sheets (DC-Fertigfolien ALUGRAM® SIL G/UV254), and the spots were visualised using UV fluorescence. Additionally, flash column chromatography was performed using silica gel (60°A pore size, 230–400 mesh, and 40–63 μm particle size) from Sigma-Aldrich under five psi compressed air. Solvents were evaporated using a Buchner rotary evaporator. Melting points were measured with an Electrothermal Digital Mel-Temp 3.0 apparatus. HPLC analysis of the synthesised compounds was conducted using a Waters Alliance e2695 equipped with a 2998 PDA detector (Waters Corporation, MA, USA), and an RP C18 column (Restek Roc, 150 × 4.6 mm, 3 μm) was employed, with a flow rate of 0.8 mL/min.

4.1.2. 2-(3-(Benzyloxy)-4-methoxyphenyl)-N-(4-fluorophenyl)imidazo [1,2-a]pyridin-3-amine (8)

A mixture of 2-aminopyridine (188 mg, 2.0 mmol) and 3-benzyloxy-4-methoxy-benzaldehyde (485 mg, 2.0 mmol) containing *p*-toluenesulfonic acid monohydrate (76 mg, 0.4 mmol) and anhydrous Na_2SO_4 (200 mg) in MeOH (10 mL), was stirred under a nitrogen atmosphere for one hour at 50 °C. Subsequently, *p*-fluorophenyl isocyanide (242 mg, 2.0 mmol) was added to the mixture. After stirring at 50 °C for 3 hrs, the mixture was cooled to room temperature and stirred overnight. Water (10 mL) was added to the reaction mixture and extracted with ethyl acetate (3 × 15 mL). The combined organic layers were washed with water (20 mL), dried over Na_2SO_4, and filtered, and the solvent was evaporated under reduced pressure. The crude product was washed with 95 % ethanol, yielding the pure product of **8** by direct precipitation (355

Table 4
Predicted ADMET properties of the tested compounds, including absorption, distribution, metabolism, excretion, and toxicity parameters.

Cmpd	TPSA, aÅ	PAINS alert	Absorption			Distribution		Excretion	Toxicity				
			Partition coefficient, Log $P_{o/w}$	Water solubility, log (mol/L)	Intestinal absorption, %(good if > 30 %)	BBB permeability, log(mol/L)	CNS permeability, log(mol/L)	Total Clearance, log(mL/min/kg)	AMES toxicity	Max. tolerated dose, log (mg/kg/day)	Hepato-toxicity	Cytotoxicity	Neuro-toxicity
8	47.79	0	5.38	-10.13	83.92	1.02	-0.72	0.64	Yes	0.11	Yes	No	Yes
9	47.00	0	4.12	-7.17	85.09	0.78	-0.94	0.71	Yes	-0.18	Yes	No	Yes
10	29.33	0	4.88	-7.98	82.88	0.67	-0.81	0.46	Yes	-0.26	No	No	Yes
11	42.47	1	3.64	-6.66	91.14	0.72	-1.51	0.68	Yes	0.03	Yes	No	Yes
12	59.54	0	4.72	-9.39	87.11	0.68	-1.47	0.44	Yes	0.03	Yes	No	Yes
13	29.33	0	5.20	-8.16	87.08	0.56	-0.92	0.86	Yes	-0.19	No	No	Yes
14	29.33	0	5.19	-9.08	83.35	0.63	-0.51	0.64	Yes	0.19	No	No	Yes
15	60.68	0	4.70	-9.75	84.41	0.62	-1.94	0.65	Yes	0.12	Yes	No	Yes
16	60.68	0	3.35	-6.79	86.26	0.34	-2.13	0.71	Yes	-0.13	Yes	No	Yes
17	58.01	0	3.54	-7.93	84.52	0.49	-1.66	0.81	Yes	0.20	Yes	No	Yes
18	42.22	0	4.12	-7.60	84.08	0.64	-0.86	0.48	Yes	-0.06	Yes	No	Yes
19	72.43	0	3.99	-9.02	87.95	-0.78	-1.70	0.45	Yes	0.08	Yes	No	Yes
20	55.36	0	2.88	-6.28	91.94	0.46	-1.93	0.69	Yes	0.08	Yes	No	Yes

mg, 40.04 %). The last step was repeated once. MP: 176.6-178°C; IR (cm^{-1}): 3212 (N-H str.), 2974 (C-H str. in CH_2), 1587 (C=C str.), 1507 (aromatic C=C str.), 1257 (C-N str.), 1220 (C-O str.), 1137 (C-F str.); ^{1}H NMR (500 MHz, $CDCl_3$) δ ppm: 7.80 (dt, *J* = 6.8, 1.2 Hz, 1H), 7.61 (dt, *J* = 9.0, 1.1 Hz, 1H), 7.57 (dd, *J* = 8.9, 2.0 Hz, 2H), 7.36 – 7.30 (m, 4H), 7.28 (dd, *J* = 6.5, 2.4 Hz, 1H), 7.20 (ddd, *J* = 9.0, 6.7, 1.3 Hz, 1H), 6.92 (t, *J* = 8.7, 5.9 Hz, 2H), 6.88 (d, *J* = 5.4 Hz, 1H), 6.76 (td, *J* = 6.8, 1.1 Hz, 1H), 6.5 (dd, *J* = 8.9, 4.2 Hz, 2H), 5.48 (s, 1H), 5.00 (s, 2H), 3.88 (s, 3H); ^{13}C NMR (126 MHz, $CDCl_3$) δ ppm: 158.0, 156.1, 149.5, 148.1, 142.6, 141.0, 139.3, 137.0, 128.4, 127.70, 127.23, 126.0, 125.0, 122.4, 120.1, 117.45, 117.38, 116.49, 116.31, 114.26, 114.20, 112.36, 112.17, 111.7, 70.5, 56.0; ^{19}F NMR (471 MHz, $CDCl_3$) δ ppm: -124.98. Anal. Calcd for $C_{27}H_{22}FN_3O_2$ (439.16) C, 73.79; H, 5.05; N 9.56; Found: C, 73.74; H, 4.90; N, 4.96.

*4.1.3. 2-(Benzo[d][1,3]dioxol-5-yl)-N-(4-fluorophenyl)imidazo[1,2-a] pyridin-3-amine (**9**)*

A mixture of 2-aminopyridine (188 mg, 2.0 mmol) and piperonal (300 mg, 2.0 mmol) containing *p*-toluenesulfonic acid monohydrate (76 mg, 0.4 mmol) and anhydrous Na_2SO_4 (200 mg) in MeOH (10 mL), was stirred under a nitrogen atmosphere for one hour at 50 °C. Next, *p*-fluorophenyl isocyanide (242 mg, 2.0 mmol) was added to the mixture, and the procedure described for **8** was followed**.** The residue was thermally crystallised with 95 % ethanol and then recrystallised using the two-solvent systems (dichloromethane:/hexane) to yield pure crystals of the title compound **9** (238 mg, 34.02 %). MP: 212.0-213.9°C; IR (cm^{-1}): 3215 (N-H str.), 2967 (C-H str. in CH_2), 1633 (C=N str.), 1573 (C=C str.), 1510 (aromatic C=C str.), 1342 (C-N str.), 1224 (C-O str.), 1036 (C-F str.); ^{1}H NMR (500 MHz, $CDCl_3$) δ ppm: 7.81 (dd, *J* = 6.7, 1.2 Hz, 1H), 7.62 (dd, *J* = 9.1, 1.1 Hz, 1H), 7.52 (dd, *J* = 7.9, 1.4 Hz, 2H), 7.23 (ddd, *J* = 9.2, 6.7, 1.3 Hz, 1H), 6.92 (t, *J* = 8.7 Hz, 2H), 6.82 (dd, *J* = 8.6, 1.2 Hz, 1H), 6.78 (td, *J* = 6.8, 1.1 Hz, 1H), 6.52 (dd, *J* = 9.0, 4.4 Hz, 2H), 5.96 (s, 2H), 5.51 (s, 1H); ^{13}C NMR (126 MHz, $CDCl_3$) δ ppm: 158.0, 156.2, 147.88, 147.39, 142.5, 140.7, 127.4, 125.1, 122.5, 121.0, 117.54, 117.36, 116.52, 116.34, 114.28, 114.22, 112.3, 108.5, 107.5, 101.0; ^{19}F NMR (471 MHz, $CDCl_3$) δ ppm: -124.91. Anal. Calcd for $C_{20}H_{14}FN_3O_2$ (347.10), C69.16; H, 4.06; N, 12.10; Found: C,69.04; H, 4.17; N, 11.98; HRMS *m/z* calcd for $C_{20}H_{14}FN_3O_2$ ($[M+H]^+$) 348.1142 found 348.1132.

*4.1.4. 2-(2,4-Difluorophenyl)-N-(4-fluorophenyl)imidazo[1,2-a]pyridin-3-amine (**10**)*

A mixture of 2-aminopyridine (188 mg, 2.0 mmol) and 2,4-difluorobenzaldehyde (284 mg, 2.0 mmol) containing $Sc(OTf)_3$ (49 mg, 0.1 mmol) and anhydrous Na_2SO_4 (200 mg) in MeOH (10 mL), was stirred under a nitrogen atmosphere for one hour at 50 °C. Next, *p*-fluorophenyl isocyanide (242 mg, 2.0 mmol) was added, and the procedure described for **8** was followed. The resultant residue was purified by flash chromatography (SiO_2, MeOH: dichloromethane: ether in 0.5:8:1.5 ratio). Further purification was achieved using preparative TLC and thermal crystallisation with 95 % ethanol, yielding the desired compound **10** (272 mg, 39.09 %). MP: 177.5-179.2°C; IR (cm^{-1}): 1625 (C=N str.), 1577 (C=C str.), 1505 (aromatic C=C str.), 1348 (C-N str.), 1210 (C-F str.); 736 (C=C bending); ^{1}H NMR (500 MHz, Chloroform-d) δ ppm: 7.83 – 7.77 (m, 2H), 7.64 (dt, *J* = 9.1, 1.1 Hz, 1H), 7.25 (ddd, *J* = 9.1, 6.7, 1.3 Hz, 1H), 6.96 – 6.91 (m, 1H), 6.87 – 6.82 (m, 3H), 6.81 (dd, *J* = 8.0, 6.7, 1.2 Hz, 1H), 6.41 (dd, *J* = 9.0, 4.3 Hz, 2H), 5.76 (d, *J* = 3.3 Hz, 1H); ^{13}C NMR (126 MHz, $CDCl_3$) δ ppm: 163.9, 163.8, 161.9, 161.8, 160.9, 160.8, 158.9, 158.8, 157.9, 156.0, 142.9, 140.7, 133.7, 132.2, 132.18, 132.15, 132.11, 125.0, 123.0, 120.4, 117.9, 116.2, 116.0, 114.6, 114.5, 112.4, 111.99, 111.96, 111.82, 111.79, 104.3, 104.1, 103.9; ^{19}F NMR (471 MHz, $CDCl_3$) δ ppm: -110.0, -110.5, -125.0.. Anal. Calcd for $C_{19}H_{12}F_3N_3$ (339.09), C, 67.25; H, 3.56; N, 12.38; Found: C, 67.39; H, 3.68; N, 12.49; HRMS *m/z* calcd for $C_{19}H_{12}F_3N_2$ ($[M+H]^+$) 340.1056 found 340.1047.

4.1.5. N-(4-fluorophenyl)-2-(furan-2-yl)imidazo[1,2-a]pyridin-3-amine (11)

A mixture of 2-aminopyridine (188 mg, 2.0 mmol) and 2-furaldehyde (193 mg, 2.0 mmol), containing $Sc(OTf)_3$ (49 mg, 0.1 mmol) and anhydrous Na_2SO_4 (200 mg) in MeOH (10 mL), was stirred under a nitrogen atmosphere for one hour at 50 °C. Next, *p*-fluorophenyl isocyanide (242 mg, 2.0 mmol) was added, and the procedure described for compound **8** was followed**.** The resultant residue was purified by flash chromatography (SiO_2, MeOH: dichloromethane: in 0.5:9.5 ratio) and then recrystallised twice from 95 % ethanol to furnish the title compound **11** (234 mg, 39.08 %). MP: 228.0-230.0°C; IR (cm^{-1}): 3348 (N-H str.), 3121 (C-H str. in =C-H), 1630 (C=N str.), 1541 (C=C str.), 1449 (aromatic C=C str.), 1354 (C-N str.), 1251 (C-O str.), 1116 (C-F str.),727 (C=C bending); ^{1}H NMR (500 MHz, Chloroform-d) δ ppm: 7.85 (td, J = 6.8, 5.6, 1.1 Hz, 1H), 7.64 (td, J = 9.1, 1.1 Hz, 1H), 7.46 (dd, J = 1.7, 0.8 Hz, 1H), 7.25-7.21 (m, 1H), 6.91 (t, J = 8.6, 1.0 Hz, 2H), 6.81 (td, J = 8.0, 6.8, 1.1 Hz, 1H), 6.76 (d, J = 3.4 Hz, 1H), 6.53 (dd, J = 8.9, 4.6 Hz, 2H), 6.45 (dd, J = 3.4, 1.7 Hz, 1H), 5.77 (s, 1H); ^{13}C NMR (126 MHz, $CDCl_3$) δ ppm: 158.2, 156.3, 142.5, 140.7, 125.4, 122.7, 118.4, 117.6, 116.3, 116.1, 115.0, 114.9, 112.6, 111.5, 108.0; ^{19}F NMR (471 MHz, $CDCl_3$) δ ppm: -124.6. Anal. Calcd for $C_{17}H_{12}FN_3O$ (293.09), C,69.62; H, 4.12; N, 14.33; Found: C, 69.51; H, 4.23; N, 14.42; HRMS *m/z* calcd for $C_{17}H_{12}FN_3O$ ($[M+H]^+$) 294.1025 found 294.1028.

4.1.6. 6-Bromo-3-(3-((4-fluorophenyl)amino)imidazo[1,2-a]pyridin-2-yl)-4H-chromen-4-one (12)

A mixture of 2-aminopyridine (188 mg, 2.0 mmol) and 6-bromo-3-formyl-chromone (506 mg, 2.0 mmol) containing $Sc(OTf)_3$ (49 mg, 0.1 mmol) and anhydrous Na_2SO_4 (200 mg) in MeOH: dichloromethane: (1:1, 10 mL), was stirred under a nitrogen atmosphere for one hour at 50 °C. Next, *p*-fluorophenyl isocyanide (242 mg, 2.0 mmol) was added, and the procedure described for compound **8** was followed**.** The resultant residue was purified by flash chromatography (SiO_2, dichloromethane: ether in a 2:8 ratio). Further purification was performed by preparative TLC, followed by thermal crystallisation with 95 % ethanol, then recrystallisation using a two-solvent system (ether/hexane) to furnish the title compound **12** (304 mg, 33.06 %). MP: 114.8-116°C; IR (cm^{-1}): 1644 (C=O str.), 1604 (C=N str.), 1556 (C=C str.), 1477 (aromatic C=C str.), 1258 (C-O str.), 1215 (C-F str.), 960 (C=C bending); ^{1}H NMR (500 MHz, Chloroform-d) δ ppm: 12.05 (d, J = 11.7 Hz, 1H), 8.34 – 8.30 (m, 2H), 8.07 (d, J = 2.5 Hz, 1H), 7.65 (td, J = 8.2, 6.3, 1.7 Hz, 1H), 7.53 (dd, J = 8.7, 2.6 Hz, 1H), 7.01 (dd, J = 7.3, 5.0 Hz, 1H), 6.91 (d, J = 8.7 Hz, 1H), 6.87 (d, J = 8.3 Hz, 1H), 5.82 (s, 1H), 3.89-3.82 (m, 1H), 3.74-3.67 (m, 1H); ^{13}C NMR (126 MHz, $CDCl_3$) δ ppm: 180.8, 155.1, 151.0, 148.5, 142.5, 138.6, 137.0, 129.1, 124.3, 120.0, 119.3, 114.6, 112.2, 104.7, 100.8, 64.0, 15.0; ^{19}F NMR (377 MHz, $CDCl_3$) δ ppm: -117.8. Anal. Calcd for $C_{22}H_{13}BrFN_3O_2$ (449.01), C, 58.69; H, 2.91; N, 9.33; Found: C, 58.81; H, 3.03; 9.18.

4.1.7. N-(4-fluorophenyl)-2-(m-tolyl)imidazo[1,2-a]pyridin-3-amine (13)

A mixture of 2-aminopyridine (188 mg, 2.0 mmol) and *m*-tolualdehyde (240 mg, 2.0 mmol), containing $Sc(OTf)_3$ (49 mg, 0.1 mmol) and anhydrous Na_2SO_4 (200 mg) in MeOH: dichloromethane: (1:1, 10 mL), was stirred under a nitrogen atmosphere for one hour at 50 °C. Next, *p*-fluorophenyl isocyanide (242 mg, 2.0 mmol) was added, and the procedure described for compound **8** was followed**.** The resultant residue was washed with cold 95 % EtOH, yielding the desired compound **13** by direct precipitation (210 mg, 33.0 %). MP: 177.6-179.3°C; IR (cm^{-1}): 1506 (aromatic C=C str.), 1344 (C-N str.), 1215 (C-F str.); 738 (C=C bending); ^{1}H NMR (500 MHz, Chloroform-d) δ ppm: 7.86 (d, J = 1.8 Hz, 1H), 7.82 (dt, J = 6.8, 1.3 Hz, 1H), 7.72 (d, J = 7.8 Hz, 1H), 7.63 (dt, J = 9.2, 1.1 Hz, 1H), 7.26 – 7.20 (m, 2H), 7.12 (d, J = 7.6 Hz, 1H), 6.91 (t, J = 8.6, 1.9 Hz, 2H), 6.78 (td, J = 6.9, 1.1 Hz, 1H), 6.52 (dd, J = 9.2, 4.3 Hz, 2H), 5.51 (s, 1H), 2.35 (s, 3H); ^{13}C NMR (126 MHz, $CDCl_3$) δ ppm: 158.0, 156.1, 142.7, 140.9, 139.5, 138.3, 133.2, 128.7, 128.5, 127.8, 125.0 123.9, 122.6, 118.2, 117.7, 116.5, 116.3, 114.4, 114.3, 112.2, 21.5; ^{19}F NMR (470 MHz, $CDCl_3$) δ ppm: -125.0. Anal. Calcd for $C_{20}H_{16}FN_3$ (317.13), C,75.69; H, 5.08; N, 13.24; Found: C, 75.57; H, 5.19; N, 13,12; HRMS *m/z* calcd for $C_{20}H_{16}FN_3$ ($[M+H]^+$) 318.1394 found 318.1390.

4.1.8. N-(4-fluorophenyl)-2-(naphthalen-2-yl)imidazo[1,2-a]pyridin-3-amine (14)

A mixture of 2-aminopyridine (188 mg, 2.0 mmol) and 2-naphthaldehyde (312 mg, 2.0 mmol), containing $Sc(OTf)_3$ (49 mg, 0.1 mmol) and anhydrous Na_2SO_4 (200 mg) in MeOH: dichloromethane: (1:1, 10 mL), was stirred under a nitrogen atmosphere for one hour at 50 °C. Next, *p*-fluorophenyl isocyanide (242 mg, 2.0 mmol) was added, and the procedure described for compound **8** was followed**.** The resultant residue was washed with cold 95 % EtOH, yielding the desired compound **14** by direct precipitation (263 mg, 37.01 %). MP: 215.6-217.0°C; IR (cm^{-1}): 3187 (N-H str.), 1572 (C=N str.), 1508 (aromatic C=C str.), 1342 (C-N str.), 1222 (C-F str.), 733 (C=C bending); ^{1}H NMR (500 MHz, Chloroform-d) δ ppm: 8.47 (d, J = 1.7 Hz, 1H), 8.10 (dd, J = 8.7, 1.8 Hz, 1H), 7.83 (dt, J = 6.8, 1.2 Hz, 1H), 7.82 – 7.77 (m, 3H), 7.66 (dt, J = 9.0, 1.2 Hz, 1H), 7.45 (dd, J = 6.2, 3.3 Hz, 2H), 7.23 (ddd, J = 9.1, 6.7, 1.3 Hz, 1H), 6.92 (t, J = 9.7 Hz, 2H), 6.78 (td, J = 8.0, 6.9, 1.1 Hz, 1H), 6.59 – 6.54 (m, 2H), 5.58 (s, 1H); ^{13}C NMR (126 MHz, $CDCl_3$) δ ppm: 158.1, 156.2, 142.9, 140.8, 139.3, 133.5, 133.0, 130.7, 128.4, 128.2, 127.6, 126.1, 125.2, 124.7, 122.6, 117.7, 116.5, 116.4, 114.4, 114.3, 112.3; ^{19}F NMR (471 MHz, $CDCl_3$) δ ppm: -124.9. Anal. Calcd for $C_{23}H_{16}FN_3$ (353.13), C,78.17; H, 4.56; N, 11.89; Found: C, 78.06; H, 4.47; N, 11,75; HRMS *m/z* calcd for $C_{23}H_{16}FN_3$ ($[M+H]^+$) 354.14010 found 354.1390.

4.1.9. 2-(3-(Benzyloxy)-4-methoxyphenyl)-N-(4-fluorophenyl)imidazo[1,2-a]pyrazin-3-amine (15)

A mixture of aminopyrazine (190 mg, 2.0 mmol) and 3-benzyloxy-4-methoxy-benzaldehyde (485 mg, 2.0 mmol) containing *p*-toluenesulfonic acid monohydrate (76 mg, 0.4 mmol) and anhydrous Na_2SO_4 (200 mg) in MeOH (10 mL), was stirred under a nitrogen atmosphere for one hour at 50 °C. Next, *p*-fluorophenyl isocyanide (242 mg, 2.0 mmol) was added, and the procedure described for compound **8** was followed**.** The resultant residue was purified by flash chromatography (SiO_2, dichloromethane: ethyl acetate in 4:6 ratio) to afford the desired compound **15** (543 mg, 61.07 %). MP: 163.2-164.4°C; IR (cm^{-1}): 3178 (N-H str.), 1610 (C=N str.), 1561 (C=C str.), 1507 (aromatic C=C str.), 1269 (C-N str.), 1221 (C-O str.), 1140 (C-F str.); ^{1}H NMR (500 MHz, $CDCl_3$) δ ppm: 9.05 (t, J = 1.2 Hz, 1H), 7.84 (dd, J = 4.6, 1.0 Hz, 1H), 7.72 (dt, J = 4.4, 1.4 Hz, 1H), 7.62 – 7.52 (m, 2H), 7.38 – 7.29 (m, 4H), 7.28 (dd, J = 5.5, 2.4 Hz, 1H), 6.94 (t, J = 8.6 Hz, 2H), 6.89 (dd, J = 8.3, 1.3 Hz, 1H), 6.48 (dd, J = 8.9, 4.3 Hz, 2H), 5.56 (s, 1H), 5.01 (s, 2H), 3.87 (s, 3H); ^{13}C NMR (126 MHz, $CDCl_3$) δ ppm: 158.3, 156.4, 150.1, 148.2, 143.2, 141.5, 140.0, 137.6, 136.7, 129.5, 128.5, 127.81, 127.22, 125.0, 120.5, 118.9, 116.69, 116.51, 115.5, 114.56, 114.50, 112.6, 111.7, 70.6, 56.0; ^{19}F NMR (377 MHz, $CDCl_3$) δ ppm: -123.88. Anal. Calcd for $C_{26}H_{21}FN_4O_2$ (440.16), C, 70.90; H, 4.81; N, 12. 72; Found: C, 70.86; H, 4.59; N, 12.80.

4.1.10. 2-(Benzo[d][1,3]dioxol-5-yl)-N-(4-fluorophenyl)imidazo[1,2-a]pyrazin-3-amine (16)

A mixture of aminopyrazine (190 mg, 2.0 mmol) and piperonal (300 mg, 2.0 mmol) containing *p*-toluenesulfonic acid monohydrate (76 mg, 0.4 mmol) and anhydrous Na_2SO_4 (200 mg) in MeOH (10 mL), was stirred under a nitrogen atmosphere for one hour at 50 °C. Next, *p*-fluorophenyl isocyanide (242 mg, 2.0 mmol) was added to the mixture, followed by the procedure described for compound **8** was followed. The resultant residue was thermally crystallised with 95 % ethanol and then recrystallised using a two-solvent system (dichloromethane:/hexane) to yield pure crystals of the title compound **16** (229 mg, 32.07 %). MP: 184.7-186.0°C; IR (cm^{-1}): 3220 (N-H str.), 2972 (C-H str. in CH_2), 1606 (C=N str.),1563 (C=C str.),) 1505 (aromatic C=C str.), 1213 (C-O str.), 1034 (C-F str.); ^{1}H NMR (400 MHz, $CDCl_3$) δ ppm: 9.08 (d, J = 1.5 Hz,

1H), 7.87 (d, $J = 4.6$ Hz, 1H), 7.75 (dd, $J = 4.5$, 1.5 Hz, 1H), 7.52 (dd, $J = 7.2$, 1.7 Hz, 2H), 6.94 (t, $J = 8.6$ Hz, 2H), 6.84 (d, $J = 8.6$ Hz, 1H), 6.52 (dd, $J = 8.9$, 4.3 Hz, 2H), 5.99 (s, 2H), 5.52 (s, 1H); ^{13}C NMR (101 MHz, $CDCl_3$) δ ppm: 158.6, 156.3, 148.1, 143.4, 141.5, 139.7, 137.6, 129.6, 126.4, 121.4, 116.77, 116.54, 115.6, 114.64, 114.56, 108.7, 107.6, 101.30; ^{19}F NMR (377 MHz, $CDCl_3$) δ ppm: -123.84. Anal. Calcd for $C_{19}H_{13}FN_4O_2$ (348.10), C, 65.51; H, 3.76; N, 16.08; Found: C, 65.63; H, 3.91; N, 15.91; HRMS *m/z* calcd for $C_{19}H_{13}FN_4O_2$ ($[M+H]^+$) 349.1095 found 349.1084.

4.1.11. N-(4-fluorophenyl)-2-(1H-indol-3-yl)imidazo[1,2-a]pyrazin-3-amine (17)

A mixture of aminopyrazine (190 mg, 2.0 mmol) and 3-Indolcarbaldehyde (290 mg, 2.0 mmol) containing $Sc(OTf)_3$ (49 mg, 0.1 mmol) and anhydrous Na_2SO_4 (200 mg) in MeOH: dichloromethane: (1:1, 10 mL), was stirred under a nitrogen atmosphere for one hour at 50 °C. Next, *p*-fluorophenyl isocyanide (242 mg, 2.0 mmol) was added, and the procedure described for compound **8** was followed. The resultant residue was purified by flash chromatography (SiO_2, MeOH: dichloromethane: Ether in 1:5:4 ratio), then crystallised from acetone to provide the title compound **17** (256 mg, 37.02 %). MP: 328.7-330.0°C; IR (cm^{-1}): 2978 (C-H str. in =C-H), 1575 (C=N str.), 1509 (aromatic C=C str.), 1351 (C-N str.), 1215 (C-F str.); 741 (C=C bending); ^{1}H NMR (500 MHz, Chloroform-*d*) δ ppm: 9.28 (s, 1H), 8.11 (t, $J = 6.7$ Hz, 2H), 7.57 (d, $J = 9.0$ Hz, 1H), 7.52 (d, $J = 2.6$ Hz, 1H), 7.36 (d, $J = 7.1$ Hz, 1H), 7.22-7.16 (m, 2H), 7.11 (t, $J = 7.9$, 1.3 Hz, 1H), 6.80 (t, $J = 6.9$ Hz, 1H), 4.04 (t, $J = 6.1$ Hz, 1H), 3.4-3.37 (m, 3H); ^{13}C NMR (126 MHz, $CDCl_3$) δ ppm: 141.5, 136.2, 131.4, 126.6, 126.2, 123.0, 122.8, 122.3, 122.0, 120.7, 120.2, 117.1, 111.32, 111.28, 110.3, 66.7, 58.0, 53.3, 44.1; ^{19}F NMR (470 MHz, $CDCl_3$) δ ppm: -114.8. Anal. Calcd for $C_{20}H_{14}FN_5$ (343.12), C, 69.96; H, 4.11; N, 20.40; Found: C, 69.73; H, 4, 23; N, 20.56; HRMS *m/z* calcd for $C_{20}H_{14}FN_5$ ($[M+H]^+$) 344.1306 found 344.1295.

4.1.12. 2-(2,4-Difluorophenyl)-N-(4-fluorophenyl)imidazo[1,2-a]pyrazin-3-amine (18)

A mixture of aminopyrazine (190 mg, 2.0 mmol) and 2,4-difluorobenzaldehyde (284 mg, 2.0 mmol) containing $Sc(OTf)_3$ (49 mg, 0.1 mmol) and anhydrous Na_2SO_4 (200 mg) in MeOH: dichloromethane: (1:1, 10 mL), was stirred under a nitrogen atmosphere for one hour at 50 °C. Next, *p*-fluorophenyl isocyanide (242 mg, 2.0 mmol) was added, and the procedure described for compound **8** was followed. The resultant residue was purified by flash chromatography (SiO_2, dichloromethane: MeOH: ether in 5:1.5:3.5 ratio), followed by preparative TLC. Then hexane was added until a yellow precipitate formed, which was finally washed with ether: hexane (1:5) to yield the desired compound **18** (216 mg, 31.05 %). MP: 151-154°C; IR (cm^{-1}): 1618 (C=N str.), 1573 (C=C str.), 1507 (aromatic C=C str.), 1350 (C-N str.), 1216 (C-F str.); ^{1}H NMR (500 MHz, Chloroform-*d*) δ ppm: 9.13 (d, $J = 1.4$ Hz, 1H), 7.90 (d, $J = 4.6$ Hz, 1H), 7.87-7.82 (m, 1H), 7.74 (dd, $J = 4.6$, 1.5 Hz, 1H), 7.01 (td, $J = 8.2$, 2.5 Hz, 1H), 6.92-6.87 (m, 3H), 6.41 (dd, $J = 9.0$, 4.3 Hz, 2H), 5.74 (d, $J = 4.1$ Hz, 1H); ^{13}C NMR (126 MHz, $CDCl_3$) δ ppm: 164.4, 164.3, 162.4, 162.3, 161.1, 161.0, 159.1, 159.0, 158.3, 156.4, 143.9, 139.5, 137.9, 135.7, 132.44, 132.40, 132.4, 132.3, 129.6, 121.9, 117.0, 116.94, 116.86, 116.83, 116.4, 116.2, 116.0, 115.13, 115.07, 112.5, 112.4, 112.28, 112.25, 104.6, 104.4, 104.2; ^{19}F NMR (471 MHz, $CDCl_3$) δ ppm: -108.4, -110.6, -123.7. Anal. Calcd for $C_{18}H_{11}F_3N4$ (340.09), C, 63.53; H, 3.26; N, 16.46; Found: C, 63.31; H, 3.47; N, 16.39.

4.1.13. 6-Bromo-3-(3-((4-fluorophenyl)amino)imidazo[1,2-a]pyrazin-2-yl)-4H-chromen-4-one (19)

A mixture of aminopyrazine (190 mg, 2.0 mmol) and 6-bromo-3-formyl-chromone (506 mg, 2.0 mmol) containing $Sc(OTf)_3$ (49 mg, 0.1 mmol) and anhydrous Na_2SO_4 (200 mg) in MeOH: dichloromethane: (1:1, 10 mL), was stirred under a nitrogen atmosphere for one hour at 50 °C. Next, *p*-fluorophenyl isocyanide (242 mg, 2.0 mmol) was added to the mixture, followed by the procedure described for compound **8.** The resultant residue was purified by crystallisation from (dichloromethane/hexane) to furnish the title compound **19** (295 mg, 32.08 %). MP: 168.0-169.8°C; IR (cm^{-1}): 3323 (N-H str.), 2972 (C-H str. in =C-H), 1649 (C=O str.), 1604 (C=N str.), 1522 (C=C str.), 1485 (aromatic C=C str.), 1360 (C-N str.), 1258 (C-O str.), 1196 (C-F str.), 794 (C=C bending), 613 (C-Br str.); ^{1}H NMR (400 MHz, Chloroform-*d*) δ ppm: 12.10 (d, $J = 11.4$ Hz, 1H), 8.33 (d, $J = 1.4$ Hz, 1H), 8.30 – 8.23 (m, 2H), 8.21 (d, $J = 11.4$ Hz, 1H), 8.07 (d, $J = 2.4$ Hz, 1H), 7.57 (dd, $J = 8.7$, 2.5 Hz, 1H), 6.95 (d, $J = 8.7$ Hz, 1H), 5.71 (s, 1H), 3.51 (s, 3H); ^{13}C NMR (101 MHz, $CDCl_3$) δ ppm: 181.4, 155.1, 147.7, 142.3, 141.3, 139.6, 137.6, 135.1, 129.2, 124.0, 120.1, 115.0, 106.4, 101.7, 55.8; ^{19}F NMR (377 MHz, $CDCl_3$) δ ppm: -117.8. Anal. Calcd for $C_{21}H_{12}BrFN_4O_2$ (450.01), C, 55.90; H, 2.68; N, 12.42; Found: C, 56.04; 2.81; N, 12.28; HRMS *m/z* calcd for $C_{21}H_{12}BrFN_4O_2$ ($[M+H]^+$) 451.0200 found 451.0194.

4.1.14. N-(4-fluorophenyl)-2-(furan-2-yl)imidazo[1,2-a]pyrazin-3-amine (20)

A mixture of aminopyrazine (190 mg, 2.0 mmol) and 2-furaldehyde (192 mg, 2.0 mmol) containing $Sc(OTf)_3$ (49 mg, 0.1 mmol) and anhydrous Na_2SO_4 (200 mg) in MeOH: dichloromethane: (1:1, 10 mL), was stirred under a nitrogen atmosphere for one hour at 50 °C. Next, *p*-fluorophenyl isocyanide (242 mg, 2.0 mmol) was added to the mixture, followed by the procedure described for compound **8.** The resultant residue was purified by flash chromatography (SiO_2, dichloromethane: MeOH: Ether in 5:1:4 ratio), followed by preparative TLC. The residue was then washed with ethyl acetate, and hexane was added dropwise until a precipitate formed, which was filtrated to furnish the title compound **20** (212 mg, 35.09 %). MP: 190.6-192.0°C; IR (cm^{-1}): 3186 (N-H str.), 1606 (C=N str.), 1555 (C=C str.), 1506 (aromatic C=C str.), 1354 (C-N str.), 1213 (C-O str.), 1022 (C-F str.), 741 (C=C bending); ^{1}H NMR (400 MHz, Chloroform-*d*) δ ppm: 9.06 (d, $J = 1.4$ Hz, 1H), 7.86 (d, $J = 4.6$ Hz, 1H), 7.72 (dd, $J = 4.5$, 1.5 Hz, 1H), 7.49 (dd, $J = 1.8$, 0.8 Hz, 1H), 6.97 – 6.89 (m, 2H), 6.84 (dd, $J = 3.4$, 0.6 Hz, 1H), 6.56 – 6.50 (m, 2H), 6.48 (dd, $J = 3.5$, 1.7 Hz, 1H), 5.89 (s, 1H); ^{13}C NMR (101 MHz, $CDCl_3$) δ ppm: 158.8, 156.4, 147.9, 143.5, 143.1, 139.6, 139.57, 137.7, 133.0, 129.7, 116.5, 116.3, 115.7, 115.53, 115.45, 111.7, 109.2; ^{19}F NMR (377 MHz, $CDCl_3$) δ ppm: -123.4. Anal. Calcd for $C_{16}H_{11}FN_4O$ (294.09), C, 65.30; H, 3.77; N, 19.04; Found: C, 65.18; H, 3.91; N, 18.91; HRMS *m/z* calcd for $C_{16}H_{11}FN_4O$ ($[M+H]^+$) 295.0989 found 295.0982.

4.2. X-ray data collection and reduction

XRD crystallographic data for compounds 9 and 20 were collected at 296 °K. Colorless, prism-like crystals were selected, mounted with epoxy on a glass fibre, and analysed at -100°C using a Gemini kappa-geometry diffractometer, specifically a Rigaku XtaLAB P200K equipped with an Atlas CCD detector. The diffraction data were processed and reduced using the CrysAlisPro program to generate an hkl file. The structures were determined by direct methods and refined using the least-squares method on F2 within the SHELXTL program package [48]. Carbon atoms were positioned computationally and refined isotropically using a riding model, while non-hydrogen atoms were refined anisotropically. Hydrogen atoms were placed in idealised positions and treated as riding models. Details of data collection and refinement are provided in Table 4.

4.3. Computational details

The molecules in the crystals are connected through intermolecular interactions, which were analysed using Hirshfeld surface analysis. This analysis involved plotting d_{norm}, shape index, curvedness, and electrostatic potential. Hirshfeld surface analysis and the generation of 2D fingerprint plots were performed using CrystalExplorer 17.5 [49]. The intermolecular interactions within the crystal were visualised on the Hirshfeld surface using a red-white-blue colour scheme [50].

The geometry optimisation procedure was executed using the

Density Functional Theory (DFT) method to obtain the coordinates that produce the minimum energy configuration of the compounds (**15-19**). Subsequently, a single-point energy calculation was performed using the optimised geometry for each molecule to generate the optimum electronic structure. Information on the energy of the frontier orbital, i.e. highest occupied molecular orbital (HOMO) and lowest unoccupied molecular orbital (LUMO), was directly extracted from the Gaussian 16 output file. GaussView 6 was used to analyse the shape of HOMO and LUMO surfaces visually. As for the choice of basis set, the triple zeta 6-311G++(d,p) set was used throughout the study. A popular DFT approach for small and medium-sized molecules in quantum chemistry computations is the B3LYP functional in conjunction with the 6–31 G(d, p) basis set because it strikes a compromise between computational economy and accuracy. This technique shows molecules' structural and dynamic characteristics [51]. The chosen basis set includes diffuse and polarisation functions that better describe the electrons' distribution within the molecule (Table 5).

The tested compounds' absorption, distribution, metabolism, excretion, and toxicity (ADMET) properties were predicted using multiple in silico tools to ensure a comprehensive evaluation. The following online platforms were utilised: SwissADME, pkCSM, Deep-PK, and ProTox-III. These web-based services were accessed to analyse key pharmacokinetic and toxicity parameters relevant to drug-likeness and anticancer activity. To assess bioavailability, SwissADME was used to predict lipophilicity (Log P), water solubility, and gastrointestinal (GI) absorption. pkCSM provided insights into intestinal absorption, blood-brain barrier (BBB) permeability, maximum tolerated dose and CNS penetration, which are crucial for evaluating compound distribution. Deep-PK was employed to estimate total clearance and metabolic stability. ProTox-III was utilised to predict hepatotoxicity, cytotoxicity, neurotoxicity, and mutagenicity (AMES toxicity test) to evaluate the safety profile of the compounds. All predictions were conducted through their respective web interfaces, and results were analysed to identify potential correlations with experimental cytotoxicity data. These in silico predictions are complementary to experimental findings, aiding in understanding pharmacokinetic behaviour and guiding future compound optimisation.

4.4. Biology

4.4.1. Anticancer activity

The cytotoxic activity of the synthesized analogues was assessed against three different cancer cell lines: human breast cancer cell line MCF-7 (ATCC number: HTB-22), the human colorectal adenocarcinoma cell line HT-29 [HTB-38; American Type Culture Collection (ATCC), Manassas, VA, USA], and the murine melanoma B16F10 [CRL-6475; American Type Culture Collection (ATCC), Manassas, VA, USA], as well as the normal cell line mouse embryonic fibroblast-1 (MEF-1; ATCC CRL-2214). All cells were cultured in high-glucose Dulbecco's Modified Eagle Medium (DMEM) that contained L-glutamine, phenol red (Fuji Film Wako, Osaka, Japan), 10 % fetal bovine serum (FBS; G.E. Healthcare, Chicago, IL, USA), and 1 % penicillin/streptomycin (P/S) (Nacalai Tesque, Kyoto, Japan). Exponentially growing cells (1×10^5 cells/well) were seeded in 24 -a 24-well plate with sterile-filtered DMEM media at 37°C under 5 % CO_2 and incubated overnight. The cells were then treated with varying concentrations of test analogues (5, 10, 50 and 100 μg/mL) and incubated for 24 h in a humidified environment. After 24 h of incubation, viable cells were counted in each well using Trypan blue exclusion test. All chemicals were first dissolved in DMSO, and the final concentration of DMSO was less than 1 % in all concentrations of the tested compounds. The IC_{50} values from at least two independent experiments were compared with the control and reported in mean ± SD. Two groups were analysed using the student's t-test, with P-values < 0.05 considered statistically significant.

Table 5
Crystal data for **9** and **20.**

Compound	9	20
CCDC	2422829	2422828
Empirical formula	$C_{20}H_{14}N_3O_2F$	$C_{16}H_{13}FN_4O_2$
Formula weight	347.34	312.30
Temperature/K	100.00	17300
Crystal system	orthorhombic	monoclinic
Space group	$P2_12_12_1$	$P2_1/c$
a/Å	5.85(10)	11.22(3)
b/Å	8.69(2)	10.13(3)
c/Å	31.07(8)	13.27(4)
α/°	90.00	90.00
β/°	90.00	104.67(3)
γ/°	90.00	90.00
Volume/Å^3	1578.15(6)	1458.62(8)
Z	4.00	4.00
ρ_{calc}g/cm^3	1.46	1.42
μ/mm^{-1}	0.10	0.11
F(000)	720.00	648.00
Crystal size/mm^3	0.19 × 0.08 × 0.02	0.12 × 0.1 × 0.02
Radiation	Mo Kα (λ = 0.71073)	Mo Kα (λ = 0.71073)
2Θ range for data collection/°	4.868 to 57.964	3.752 to 59.418
Index ranges	$-7 \le h \le 7$, $-10 \le k \le 11$, $-41 \le l \le 38$	$-14 \le h \le 13$, $-13 \le k \le 12$, $-18 \le l \le 17$
Reflections collected	34152.00	31014.00
Independent reflections	3783 [R_{int} = 0.0412, R_{sigma} = 0.0249]	3655 [R_{int} = 0.0344, R_{sigma} = 0.0239]
Data/restraints/parameters	3783/1/239	3655/3/220
Goodness-of-fit on F^2	1.062	1.049
Final R indexes [I≥2σ (I)]	R_1 = 0.0310, wR_2 = 0.0742	R_1 = 0.0386, wR_2 = 0.0905
Final R indexes [all data]	R_1 = 0.0362, wR_2 = 0.0762	R_1 = 0.0544, wR_2 = 0.0960
Largest diff. peak/hole / e Å^{-3}	0.18/-0.22	0.19/-0.22

CRediT authorship contribution statement

Isra' Al-Qadi: Formal analysis, Investigation, Methodology, Writing – original draft, Writing – review & editing. **Michel Hanania:** Resources, Supervision, Validation, Writing – original draft, Writing – review & editing. **Saied M Soliman:** Software, Writing – original draft, Writing – review & editing. **Nurul Izzaty Hassan:** Software, Writing – review & editing. **Wan Nurfadhilah Zaharim:** Software, Writing – review & editing. **Saki Raheem:** Project administration, Software, Supervision, Validation, Visualization, Writing – original draft, Writing – review & editing. **Nawaf Al-Maharik:** Formal analysis, Investigation, Methodology, Project administration, Supervision, Visualization, Writing – original draft, Writing – review & editing.

Declaration of competing interest

The authors declare that they have no known competing financial interests or personal relationships that could have appeared to influence the work reported in this paper.

Supplementary materials

Supplementary material associated with this article can be found, in the online version, at doi:10.1016/j.molstruc.2025.142549.

Data availability

Data will be made available on request.

References

[1] J. Ferlay, M. Colombet, I. Soerjomataram, D.M. Parkin, M. Piñeros, A. Znaor, et al., Cancer statistics for the year 2020: an overview, Int. J. Cancer 149 (2021) 778–789, https://doi.org/10.1002/ijc.33588.

[2] K. Azijli, E. Stelloo, G.J. Peters, A.J.M. Van Den Eertwegh, New developments in the treatment of metastatic melanoma: immune checkpoint inhibitors and targeted therapies, Anticancer Res. 34 (2014) 1493–1505.

[3] S. Nisar, T. Masoodi, K.S. Prabhu, S. Kuttikrishnan, L. Zarif, S. Khatoon, S. Ali, S. Uddin, A.A. Akil, M. Singh, M.A. Macha, Natural products as chemo-radiation therapy sensitizers in cancers, Biomed. Pharmacother. 154 (2022) 113610, https://doi.org/10.1016/j.biopha.2022.113610.

[4] R. Kaur, A. Bhardwaj, S. Gupta, Cancer treatment therapies: traditional to modern approaches to combat cancers, Mol. Biol. Rep. 50 (2023) 9663–9676, https://doi.org/10.1007/s11033-023-08809-3.

[5] L. Yang, P. Shi, G. Zhao, J. Xu, W. Peng, J. Zhang, G. Zhang, X. Wang, Z. Dong, F. Chen, H. Cui, Targeting cancer stem cell pathways for cancer therapy, Signal Transduct. Target. Ther. 5 (2020) 8, https://doi.org/10.1038/s41392-020-0110-5.

[6] B. Cesur-Ergün, D. Demir-Dora, Gene therapy in cancer, J. Gene Med. 25 (2023) e3550, https://doi.org/10.1002/jgm.3550.

[7] S. Gavas, S. Quazi, T.M. Karpiński, Nanoparticles for cancer therapy: current progress and challenges, Nanoscale Res. Lett. 16 (2021) 173, https://doi.org/10.1186/s11671-021-03628-6.

[8] L. Sun, H. Liu, Y. Ye, Y. Lei, R. Islam, S. Tan, R. Tong, Y.B. Miao, L. Cai, Smart nanoparticles for cancer therapy, Signal Transduct. Target. Ther. 8 (2023) 418, https://doi.org/10.1038/s41392-023-01642-x.

[9] A. Kamal, G.B. Kumar, V.L. Nayak, V.S. Reddy, A.B. Shaik, M.K. Reddy, Design, synthesis and biological evaluation of imidazopyridine/imidazopyrimidine-benzimidazole conjugates as potential anticancer agents, Medchemcomm 6 (2015) 606–612, https://doi.org/10.1039/C4MD00400K.

[10] S. Muniyan, Y.W. Chou, M.A. Ingersoll, A. Devine, M. Morris, V.A. Odero-Marah, S. A. Khan, W.G. Chaney, X.R. Bu, M.F. Lin, Antiproliferative activity of novel imidazopyridine derivatives on castration-resistant human prostate cancer cells, Cancer Lett. 353 (2014) 59–67, https://doi.org/10.1016/j.canlet.2014.07.002.

[11] S. Aliwaini, A.M. Awadallah, R.Y. Morjan, M. Ghunaim, H. Alqaddi, A. Y. Abuhamad, E.A. Awadallah, Y.M. Abughefra, Novel imidazo [1, 2a] pyridine inhibits AKT/mTOR pathway and induces cell cycle arrest and apoptosis in melanoma and cervical cancer cells, Oncol. Lett. 18 (2019) 830–837, https://doi.org/10.3892/ol.2019.10341.

[12] O. Kim, Y. Jeong, H. Lee, S.S. Hong, S. Hong, Design and synthesis of imidazopyridine analogues as inhibitors of phosphoinositide 3-kinase signaling and angiogenesis, J. Med. Chem. 54 (2011) 2455–2466, https://doi.org/10.1021/jm101582z.

[13] Y.H. Fan, W. Li, D.D. Liu, M.X. Bai, H.R. Song, Y.N. Xu, S. Lee, Z.P. Zhou, J. Wang, H.W. Ding, Design, synthesis, and biological evaluation of novel 3-substituted imidazo [1, 2-a] pyridine and quinazolin-4 (3H)-one derivatives as PI3Kα inhibitors, Eur. J. Med. Chem. 139 (2017) 95–106, https://doi.org/10.1016/j.ejmech.2017.07.074.

[14] A.T. Baviskar, C. Madaan, R. Preet, P. Mohapatra, V. Jain, A. Agarwal, S. K. Guchhait, C.N. Kundu, U.C. Banerjee, P.V. Bharatam, N-fused imidazoles as novel anticancer agents that inhibit catalytic activity of topoisomerase IIα and induce apoptosis in G1/S phase, J. Med. Chem. 54 (2011) 5013–5030, https://doi.org/10.1021/jm200235u.

[15] U.P. Yadav, A.J. Ansari, S. Arora, G. Joshi, T. Singh, H. Kaur, N. Dogra, R. Kumar, S. Kumar, D.M. Sawant, S. Singh, Design, synthesis and anticancer activity of 2-arylimidazo [1, 2-a] pyridinyl-3-amines, Bioorg. Chem. 118 (2022) 105464, https://doi.org/10.1016/j.bioorg.2021.105464.

[16] R. Garamvoelgyi, J. Dobos, A. Sipos, S. Boros, E. Illyes, F. Baska, L. Kekesi, I. Szabadkai, C. Szantai-Kis, G. Kéri, L. Őrfi, Design and synthesis of new imidazo [1, 2-a] pyridine and imidazo [1, 2-a] pyrazine derivatives with antiproliferative activity against melanoma cells, Eur. J. Med. Chem. 108 (2016) 623–643, https://doi.org/10.1016/j.ejmech.2015.12.001.

[17] M.A. Ismail, R. Brun, T. Wenzler, F.A. Tanious, W.D. Wilson, D.W. Boykin, Novel dicationic imidazo [1, 2-a] pyridines and 5, 6, 7, 8-tetrahydro-imidazo [1, 2-a] pyridines as antiprotozoal agents, J. Med. Chem. 47 (2004) 3658–3664, https://doi.org/10.1021/jm0400092.

[18] A. Gueiffier, S. Mavel, M. Lhassani, A. Elhakmaoui, R. Snoeck, G. Andrei, O. Chavignon, J.C. Teulade, M. Witvrouw, J. Balzarini, E. De Clercq, Synthesis of imidazo [1, 2-a] pyridines as antiviral agents, J. Med. Chem. 41 (1998) 5108–5112, https://doi.org/10.1021/jm981051y.

[19] T.H. Al-Tel, R.A. Al-Qawasmeh, R. Zaarour, Design, synthesis and in vitro antimicrobial evaluation of novel imidazo [1, 2-a] pyridine and imidazo [2, 1-b][1, 3] benzothiazole motifs, Eur. J. Med. Chem. 46 (2011) 1874–1881, https://doi.org/10.1016/j.ejmech.2011.02.051.

[20] L. Dymińska, Imidazopyridines as a source of biological activity and their pharmacological potentials—infrared and Raman spectroscopic evidence of their content in pharmaceuticals and plant materials, Bioorg. Med. Chem. 23 (2015) 6087–6099, https://doi.org/10.1016/j.bmc.2015.07.045.

[21] N. Devi, D.K. Singh, R. Rawal, J. Bariwal, V. Singh, Medicinal attributes of imidazo [1, 2-a] pyridine derivatives: an update, Curr. Top. Med. Chem. 16 (2016) 2963–2994, https://doi.org/10.2174/1568026616666160506145539.

[22] Y. Qian, Y. Zhang, P. Zhong, K. Peng, Z. Xu, X. Chen, K. Lu, G. Chen, X. Li, G. Liang, Inhibition of inflammation and oxidative stress by an imidazopyridine derivative X22 prevents heart injury from obesity, J. Cell. Mol. Med. 20 (2016) 1427–1442, https://doi.org/10.1111/jcmm.12832.

[23] A. Boltjes, A. Dömling, The Groebke-Blackburn-Bienaymé reaction, Eur. J. Org. Chem. 2019 (2019) 7007–7049, https://doi.org/10.1002/ejoc.201901124.

[24] A.K. Bagdi, S. Santra, K. Monir, A. Hajra, Synthesis of imidazo [1, 2-a] pyridines: a decade update, Chem. Commun. 51 (2015) 1555–1575, https://doi.org/10.1039/C4CC08495K.

[25] D.J. Zhu, J.X. Chen, M.C. Liu, J.C. Ding, H.Y. Wu, Catalyst: and solvent-free synthesis of imidazo [1, 2-a] pyridines, J. Braz. Chem. Soc. 20 (2009) 482–487, https://doi.org/10.1590/S0103-50532009000300012.

[26] Y.Y. Xie, Z.C. Chen, Q.G. Zheng, Organic reactions in ionic liquids: ionic liquid-accelerated cyclocondensation of α-tosyloxyketones with 2-aminopyridine, Synth 2002 (2002) 1505–1508, https://doi.org/10.1055/s-2002-33330.

[27] J.S. Yadav, B.S. Reddy, Y.G. Rao, M. Srinivas, A.V. Narsaiah, Cu (OTf) 2-catalyzed synthesis of imidazo [1, 2-a] pyridines from α-diazoketones and 2-aminopyridines, Tetrahedron. Lett. 48 (2007) 7717–7720, https://doi.org/10.1016/j.tetlet.2007.08.090.

[28] D.K. Nair, S.M. Mobin, I.N. Namboothiri, Synthesis of imidazopyridines from the Morita–Baylis–Hillman acetates of nitroalkenes and convenient access to Alpidem and Zolpidem, Org. Lett. 14 (2012) 4580–4583, https://doi.org/10.1021/ol3020418.

[29] K. Groebke, L. Weber, F. Mehlin, Synthesis of imidazo [1, 2-a] annulated pyridines, pyrazines and pyrimidines by a novel three-component condensation, Synlett 1998 (1998) 661–663.

[30] C. Blackburn, B. Guan, P. Fleming, K. Shiosaki, S. Tsai, Parallel synthesis of 3-aminoimidazo [1, 2-a] pyridines and pyrazines by a new three-component condensation, Tetrahedron. Lett. 39 (1998) 3635–3638, https://doi.org/10.1016/S0040-4039(98)00653-4.

[31] H. Bienayme, K. Bouzid, A new heterocyclic multicomponent reaction for the combinatorial synthesis of fused 3-aminoimidazoles, Angew. Chem. Int. Ed. 37 (1998) 2234–2237, https://doi.org/10.1002/(SICI)1521-3773(19980904)37:16<2234::AID-ANIE2234>3.0.CO;2-R.

[32] A.J. Buckmelter, L. Ren, E.R. Laird, B. Rast, G. Miknis, S. Wenglowsky, S. Schlachter, M. Welch, E. Tarlton, J. Grina, J. Lyssikatos, The discovery of furo [2, 3-c] pyridine-based indanone oximes as potent and selective B-Raf inhibitors, Bioorg. Med. Chem. Lett. 21 (2011) 1248–1252, https://doi.org/10.1016/j.bmcl.2010.12.039.

[33] M.Z. Hernandes, S.M. Cavalcanti, D.R. Moreira, W.F. de Azevedo Junior, A.C. Leite, Halogen atoms in the modern medicinal chemistry: hints for the drug design, Curr. Drug Targets 11 (2010) 303–314, https://doi.org/10.2174/138945010790711996.

[34] J. Ren, M. Yang, H. Liu, D. Cao, D. Chen, J. Li, L. Tang, J. He, Y.L. Chen, M. Geng, B. Xiong, Multi-substituted 8-aminoimidazo [1, 2-a] pyrazines by Groebke–Blackburn–Bienaymé reaction and their Hsp90 inhibitory activity, Org. Biomol. Chem. 13 (2015) 1531–1535, https://doi.org/10.1039/C4OB01865F.

[35] J. Volaric, W. Szymanski, N.A. Simeth, B.L. Feringa, Molecular photoswitches in aqueous environments, Chem. Soc. Rev. 50 (2021) 12377–12449, https://doi.org/10.1039/D0CS00547A.

[36] S. Hamadouche, H. Merouani, O. Aidat, N. Ouddai, B. Ernst, M. Alam, Y. Benguerba, Theoretical design of new grafted molecule d-glucosamine-oxyresveratrol-essential amino acids: DFT evaluation of the structure-antioxidant activity, ACS Omega 9 (2024) 37128–37140, https://doi.org/10.1021/acsomega.4c04356.

[37] K.M. Hutchins, Functional materials based on molecules with hydrogen-bonding ability: applications to drug co-crystals and polymer complexes, R. Soc. Open. Sci. 5 (2018) 180564, https://doi.org/10.1098/rsos.180564.

[38] H. Saluja, A. Mehanna, R. Panicucci, E. Atef, Hydrogen bonding: between strengthening the crystal packing and improving solubility of three haloperidol derivatives, Molecules 21 (2016) 719, https://doi.org/10.3390/molecules21060719.

[39] E.A. Meyer, R.K. Castellano, F. Diederich, Interactions with aromatic rings in chemical and biological recognition, Angew. Chem. Int. Edit. 42 (2003) 1210–1250, https://doi.org/10.1002/anie.200390319.

[40] S. Suda, A. Tateno, D. Nakane, T. Akitsu, Hirshfeld surface analysis for investigation of intermolecular interaction of molecular crystals, Int. J. Org. Chem. (Irvine) 13 (2023) 57–85, https://doi.org/10.4236/ijoc.2023.132006.

[41] M. Miar, A. Shiroudi, K. Pourshamsian, A.R. Oliaey, F. Hatamjafari, Theoretical investigations on the HOMO-LUMO gap and global reactivity descriptor studies, natural bond orbital, and nucleus-independent chemical shifts analyses of 3-phenylbenzo [d] thiazole-2 (3-H)-imine and its para-substituted derivatives: solvent and substituent effects, J. Chem. Res. 45 (2021) 147–158, https://doi.org/10.1177/1747519820932013.

[42] N. Blankevoort, P. Bastante, R.J. Davidson, R.J. Salthouse, A.H. Daaoub, P. Cea, S. M. Solans, A.S Batsanov, S. Sangtarash, M.R. Bryce, N. Agrait, Exploring the impact of the HOMO-LUMO gap on molecular thermoelectric properties: a comparative study of conjugated aromatic, quinoidal, and donor-acceptor core systems, ACS Omega 9 (2024) 8471–8477, https://doi.org/10.1021/acsomega.3c0970.

[43] M. Jafari, E. Ghadami, T. Dadkhah, H. Akhavan-Niaki, PI3k/AKT signaling pathway: erythropoiesis and beyond, J. Cell. Physiol. 234 (2019) 2373–2385, https://doi.org/10.3892/mmr.2018.9713.

[44] F. Peytam, Z. Emamgholipour, A. Mousavi, M. Moradi, R. Foroumadi, L. Firoozpour, F. Divsalar, M. Safavi, A. Foroumadi, Imidazopyridine-based kinase inhibitors as potential anticancer agents: a review, Bioorg. Chem. (2023) 106831, https://doi.org/10.1016/j.bioorg.2023.106831.

[45] R. Krishnamoorthy, P. Anaikutti, Iodine catalyzed synthesis of imidazo[1,2-a] pyrazine and imidazo[1,2-a]pyridine derivatives and their anticancer activity, RSC Adv. 13 (2023) 36439–36454, https://doi.org/10.1039/D3RA07842F.

[46] S. Myadaraboina, M. Alla, V. Saddanapu, V.R. Bommena, A. Addlagatta, Structure activity relationship studies of imidazo[1,2-a]pyrazine derivatives against cancer cell lines, Eur. J. Med. Chem. 45 (2010) 5208–5216, https://doi.org/10.1016/J.EJMECH.2010.08.035.

[47] S. Zhan, Y. Zhang, T. Cao, R. Yang, Q. Wang, L. Huang, R. Cui, J. Yu, H. Meng, Y. Wang, S. Zhang, M. Zheng, X. Wu, Discovery of imidazo[1,2-a]pyrazine derivatives as potent ENPP1 inhibitors, J. Med. Chem. 67 (2024) 18317–18333, https://doi.org/10.1021/ACS.JMEDCHEM.4C01634.

[48] Agilent Technologies, CrysAlisPro, Version 1.171.36.20. data collection and processing software for agilent X-ray diffractometers. Agilent Technologies 2013. https://www.agilent.com/cs/library/usermanuals/Public/CrysAlis_Pro_User_Manual.pdf. (Accessed 18 December 2024).

[49] M.J. Turner, J.J. McKinnon, S.K. Wolff, D.J. Grimwood, P.R. Spackman, D. Jayatilaka, M.A. Spackman, Crystal Explorer17, University of Western Australia, 2017. http://hirshfeldsurface.net.

[50] J.J. McKinnon, D. Jayatilaka, M.A. Spackman, Towards quantitative analysis of intermolecular interactions with Hirshfeld surfaces, Chem. Commun. 37 (2007) 3814–3816, https://doi.org/10.1039/B704980C.

[51] M. Azzouzi, Z. EI Ouafi, O. Azougagh, W. Daoudi, H. Ghazal, S. EI Barkany, R. Abderrazak, S. Mazières, A. EI Aatiaoui, A. Oussaid, Design, synthesis, and computational studies of novel imidazo[1,2-a]pyrimidine derivatives as potential dual inhibitors of hACE2 and spike protein for blocking SARS-CoV-2 cell entry, J. Mol. Struct. 1285 (2023) 135525, https://doi.org/10.1016/J.MOLSTRUC.2023.135525.